MEENAKUMARI, H.N.R., ZANGANEH, H. and HOSSAIN, M. 2024. Effect of slug characteristics on the nonlinear dynamic response of a long flexible fluid-conveying cylinder. *Applied ocean research* [online], 147, article number 103978. Available from: https://doi.org/10.1016/j.apor.2024.103978

Effect of slug characteristics on the nonlinear dynamic response of a long flexible fluid-conveying cylinder.

MEENAKUMARI, H.N.R., ZANGANEH, H. and HOSSAIN, M.

2024

© 2024 The Author(s). Published by Elsevier Ltd. This is an open access article under the CC BY license (http://creativecommons.org/licenses/by/4.0/).

OpenAIR @RGU

This document was downloaded from https://openair.rgu.ac.uk

Applied Ocean Research 147 (2024) 103978

Contents lists available at ScienceDirect

Applied Ocean Research

journal homepage: www.elsevier.com/locate/apor

Effect of slug characteristics on the nonlinear dynamic response of a long flexible fluid-conveying cylinder

Hareesh Narain Ravindran Meenakumari, Hossein Zanganeh *, Mamdud Hossain *

School of Engineering, Robert Gordon University, Garthdee, Aberdeen AB10 7JG, United Kingdom

ARTICLE INFO

Keywords:
Slug liquid-gas flow
Flexible cylinder
3-D response
Nonlinear dynamics
Fluid-structure interaction

ABSTRACT

Hydrocarbon flows in a marine riser may appear in multiple phases with varying flow patterns, among which, slug flows are known to exhibit complex flow characteristics due to fluctuations in multiphase mass, velocities, and pressure changes. Bulk of the literature concerning internal single and two-phase flow induced vibrations have largely focused on the use of a linearized tension beam model. In this study, the fluid-structure interaction phenomena of a submerged long flexible cylinder conveying two-phase slug flows is investigated taking into account the geometric and hydrodynamic nonlinearities. A semi-empirical theoretical model which consists of nonlinear structural equations of coupled out-of-plane, in-plane and axial structural motions is presented for the analysis and prediction of two-phase slug flow induced vibrations (SIV). The model includes equations involving centrifugal and Coriolis forces to capture mass variations in the slug flow regime. A numerical space-time finite difference approach combined with a frequency domain analysis is used for analyzing the highly nonlinear three-dimensional responses. The model assumes constant geometric properties across the span of the cylinder and utilizes an idealized slug unit concept, wherein slug properties are considered to be fully developed and undisturbed by pipe oscillations. Model validations are performed through comparisons with published experimental internal flow-induced vibration results. Parametric study captures the effects of several key slug characteristics on the vibration responses of a fluid-conveying cylinder. The results demonstrate amplitude-modulation response, mean displacements, three-dimensional cylinder displacements due to geometric nonlinear couplings and the influence of internal flow velocities. Higher dominant modes and oscillation frequencies were observed when the cylinder experiences large amplitude motions at specific slug formations. A new dimensionless parameter is introduced to predict scenarios of high amplitude oscillations for long flexible cylinders carrying two-phase slug flows.

1. Introduction

In the last few decades, the abundant growth in energy demands and the depletion of hydrocarbon sources in shallow waters have led oil and gas industry pioneers explore hydrocarbon reserves in deep-water oceans. One main component used during oil and gas production in deep-water oceans are marine risers, which are long flexible cylindrical structures providing a link between the subsea wells and the offshore floating unit (Mohmmeda et al., 2019). Due to its flexible nature and high aspect (length-to-diameter) ratio, risers can undergo significant flow-induced vibrations (FIV) when exposed to unavoidable environmental loads such as currents, waves, and internal flow. Transportation of hydrocarbons in marine risers mostly occurs in multiple phases, as simultaneous flow of gas, liquid and solids or a combination of the two (Ehinmowo and Cao, 2015). Depending on the pipe-flow properties and phase interaction characteristics, several flow patterns may emerge. This in turn can lead to complex hydrodynamic behaviour because of various space-time varying multiphase flow variables. Of the various multiphase flow regimes, the slug flow regime may induce large vibrations and cyclic stresses along the pipeline due to chaotic fluctuations in mass distributions and pressure variations (Mohmmeda et al., 2019). Recently, Khan et al. (2022) presented a comprehensive review of two-phase flow-induced vibration. The review reported that most of the literature acknowledges that significant vibrations occur for straight pipes and pipes with bends during slug or churn flow regimes. In practice, many accidents have been reported with the primary cause identified as vibrations due to internal flow. Slug liquid accumulation in a steam pipeline of a chemical plant resulted in a rupture accident due to

* Corresponding authors.
E-mail addresses: h.zanganeh@rgu.ac.uk (H. Zanganeh), m.hossain@rgu.ac.uk (M. Hossain).

https://doi.org/10.1016/j.apor.2024.103978
Received 1 December 2023; Received in revised form 19 March 2024; Accepted 19 March 2024
Available online 27 March 2024
0141-1187/© 2024 The Author(s). Published by Elsevier Ltd. This is an open access article under the CC BY license (http://creativecommons.org/licenses/by/4.0/).

excessive pressure increase (Gong, 2010). Zaldivar (2014) recorded a failure in the riser section due to cyclic stresses on the pipeline conveying two-phase slug flows.

Over the years, the effect of internal multiphase flow has been ignored with researchers more focused on the dynamics of a riser due to external loads such as ocean currents and waves. However, in the recent past, several theoretical and numerical approaches have been employed by researchers to better understand the dynamics of internal flow-induced vibrations. These approaches involve the development of mathematical models and the use of computational fluid dynamics techniques. Griffith (1984) observed the mechanism whereby mass fluctuations in densities were noticed during slug flow which led to vibrations in a riser when the structure natural frequency was close to the fluctuation frequencies. Moe and Chucheepsakul (1988) investigated the effect of internal single-phase fluid through a vertical riser and noticed that the natural frequencies decreased as the internal flow velocities increased. The authors also noticed structural instabilities at specific internal flow velocities during the slug flow regime.

Patel and Syed (1989) investigated the effects of internal slug flow on the response of flexible marine risers. A numerical model comprising dynamic excitation due to fluctuating internal mass was developed and compared with results from experimental arrangements. The study showed high internal pressures due to two-phase slug flows can induce large displacements and lead to cyclic stresses on the system. Wu and Lou (1991) developed a mathematical model to analyse the lateral motion of a marine riser conveying internal flow. The study concluded that the displacements and bending stress are sensitive to bending stiffness and that stiffness becomes an influencing parameter in the dynamic response at high internal flow velocities. Monette and Pettigrew (2004) studied the fluid elastic instability behaviour of vertical cylinders under internal two-phase flow and modified the existing theoretical model, which was originally developed for single-phase flows. Monprapurson et al. (2006) studied the effects of internal pulsatile flow on the static and dynamic response of an extensible flexible marine riser. Results from the study revealed that internal flow accelerations could displace vibrational equilibrium positions of the marine riser and fluctuations in internal flow cause large amplitude displacements and a decrease in natural frequencies.

A free vibration natural frequency analysis was performed by Henandez et al. (2014) on a marine riser transporting internal multiphase flow. The study demonstrated the contributions of centrifugal and Coriolis forces to the dynamic behaviour of the riser as internal flow velocity increases. Slug flow induced vibrations (SIV) of a steel lazy wave marine riser was studied by Miranda and Paik (2019) using a space-time varying rectangular pulse train mass. The study observed vibration frequencies excited at slug frequencies. During low slug frequencies and long liquid slugs the amplitude of motion was found to be large and vice-versa during high slug frequencies and short liquid slugs. Jia (2012) investigated the SIV phenomenon in a pipeline span, jumper and riser section using computation fluid dynamics approach. Numerical results presented insights into the process of slug formation and decay in conjunction with pipe displacements due to slug flow. In a following study, Jia (2013) analysed the effect of different boundary conditions, flow rates, slug lengths and slug frequencies on the dynamic response of a straight horizontal pipe. Slug-induced vibrations were found to be the highest at higher liquid flow rates and long slug lengths.

Moreover, experimental investigations have also been performed to understand two-phase flow-induced vibration problems. Experiment studies on slug flow induced vibrations of straight pipes have been performed by few researchers. The effect of superficial velocities on the vibration responses of a horizontal pipe conveying air-water slug flows was conducted by Al-Hashimy et al. (2016). Vibration response amplitudes were noticed to increase gradually with increase in liquid superficial velocities at fixed gas superficial velocities, whilst oscillation frequencies decreased with increase in liquid superficial velocities. Additionally, pipe displacements increased up to 64 % when liquid superficial velocities increased from 0.65 m/s to 1 m/s. Wang et al. (2018) validated the developed semi-empirical model using in-house experiments to investigate the effect different slug flow characteristics such as liquid slug lengths (L_S), and translational velocities (V_t). Oscillations due to two-phase slug flows were found to be due to sudden changes in the structure mass, stiffness and loading when liquid slugs pass through the system indicating the significant influence of centrifugal and Coriolis force on the dynamic response of the structure. Vibration responses were also noticed to be large when the longest slug passed through the system.

In addition, experiments on catenary shaped cylinders have also been conducted. Bordalo et al. (2008) conducted laboratory experiments to study the influence of internal two-phase flow on the vibration responses of a catenary riser. The investigation observed the riser response to annular and slug flow patterns and showed that large oscillation amplitudes occur during the slug flow regime when compared to annular flows. A series of laboratory experiments were carried out by Zhu et al. (2018a) for small-diameter tubes to investigate SIV of a free hanging catenary riser. Superficial velocities of liquid and gas were varied from 0.1 m/s to 0.6 m/s and 0.06 m/s to 0.3 m/s respectively. During low liquid superficial velocities severe slugging were noticed with liquid slug lengths smaller than the length of the pipe. As liquid superficial velocities increase, varying slug lengths and chaotic oscillations were noticed. In a further study Zhu et al. (2018b) observed that at higher gas-liquid ratios multi-mode oscillation responses were noticed while at lower mixture velocities, accumulation of longer liquid slugs lead to high oscillation amplitudes. With an increase in mixture velocities, the accumulation of long liquid slugs appeared to be difficult due to the increase in gas superficial velocities.

The bulk of the literature concerning flow-induced vibrations has primarily focused on the structural dynamics of a riser subjected to external hydrodynamic loads, such as vortex-induced vibrations, with few studies addressing internal two-phase flow-induced vibrations. Furthermore, literature on two-phase flow-induced vibrations has predominantly utilized a simplified linearized tensioned beam model. Fundamental understanding of the SIV phenomena in three-dimensional (3-D) space and time considering in-line and axial dynamics remains limited. Therefore, this study takes into account the geometric and hydrodynamic nonlinearities to address limitations in the SIV model and presents a three-dimensional vibration prediction model for the analysis of two-phase slug flow induced vibrations of a long flexible cylinder. Moreover, this study employs an idealized slug unit concept through a rectangular pulse train model, presuming fully developed slug flow properties that remain unaffected by pipe oscillations. Additionally, the slug flow model is considered time varying, maintaining constant flow properties as it passes through cylinder.

This paper is structured as follows. In Section 2, a system of dimensional and dimensionless nonlinear equations capable of predicting vibrations due to internal two-phase slug flows are presented along with external nonlinear hydrodynamic forces. In Section 3, the developed 3-D SIV model is validated with experimental comparisons. Results from a parametric study analyzing the effect of slug characteristics on the dynamic response of a vertical straight cylinder are presented in Section 4. The paper ends with the conclusions in Section 5.

2. Three-dimensional SIV phenomenological model

Marine risers with high aspect (length-to-diameter, L/D) ratios are commonly utilized for deep-water explorations, making them prone to high amplitude oscillations caused by both external hydrodynamic loads and internal multiphase flows. Fig. 1 depicts the schematic model of long flexible cylinder in a fixed global Cartesian ($X-Y-Z$) system subjected to internal two-phase slug flow traversing through the cylinder and single-phase external flow. The cylinder in this study is considered to be vertical and fully submerged with two-phase internal flows in the axial direction. Two different conditions of the riser are

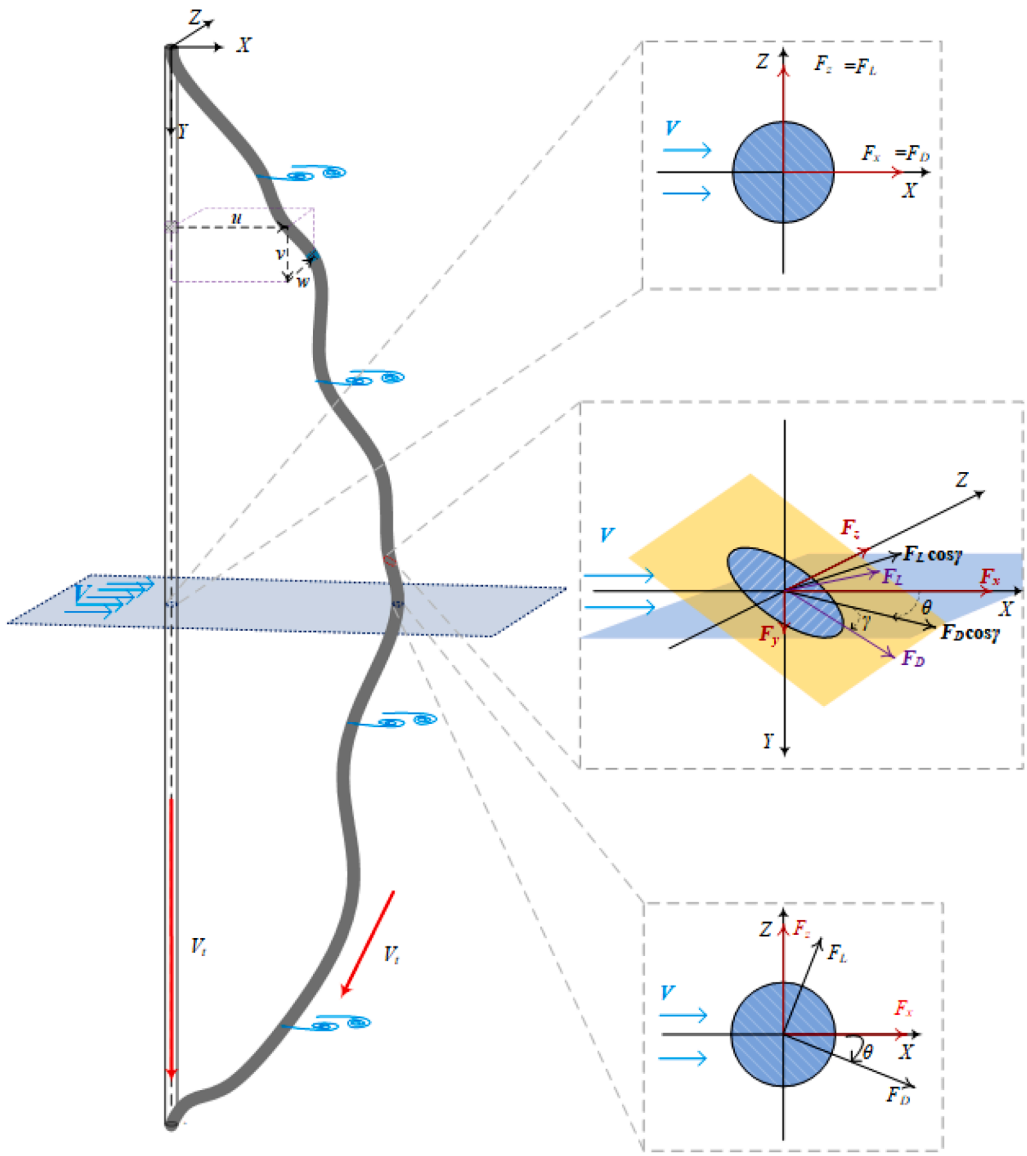

Fig. 1. Schematic 3-D model of a flexible cylinder subjected to external loads and internal two-phase slug flows.

described, the initial equilibrium state subjected to internal loading and the dynamic response configuration experiencing travelling internal slug flows from a static equilibrium in the vertical direction. The flexible cylinder is assumed to be linearly elastic with constant Young's modulus (E) and have uniform structural properties such as mass per unit length (m), still water added mass ($m_a = \rho\pi D^2/4$ with ρ being external fluid density, per length (L), mass of internal fluid (m_f), per length (L), diameter (D), bending stiffness (EI), axial stiffness (EA_r), cross-sectional area (A_r), damping coefficient (c) and moment of Inertia (I). The cylinder is capable of further displacements in the X direction due to nonlinear coupling terms in the equation. Also, for realistic predictions of SIV for offshore operations, it is crucial to take into consideration 3-D vibration response and geometric nonlinearities (Zanganeh and Srinil, 2016). Fig. 2 illustrates the application of the slug unit cell concept in this study originally introduced by Wallis (1969). In this concept, one slug unit is divided into a liquid phase (slug holdup, H_{LS}) containing

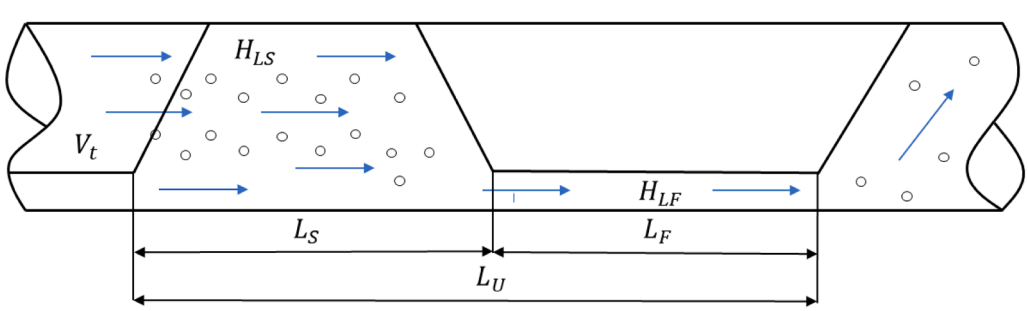

Fig. 2. Schematic view of an idealized slug unit cell.

small gas bubbles, along with a gas phase over a thin liquid film (H_{LF}), passing through the cylinder with a translational velocity, V_t. The travelling slug liquid holdup and liquid film experience shear stresses at the gas-wall, liquid-wall or liquid-gas interfaces. The slug liquid holdup is assumed to completely fill the cross-section of the cylinder over a length L_S, while the thin film liquid holdup partially occupies the cross-section over a length L_F. Together, these lengths constitute one slug unit with a total length L_U.

2.1. Three-dimensional nonlinear structural model

The partial-differential equations of the riser response satisfying the Euler-Bernoulli beam hypothesis in three-dimensional space and time in general dimensional form can be expressed as (Hara, 1973; Srinil et al., 2009; Zanganeh and Srinil, 2016):

$$\begin{aligned}&(m+m_a+m_f)\ddot{u}+c\dot{u}+EIu^{(IV)}+2m_fV_t\dot{u}'+m_fV_t^{2u''}+\Big(\dot{m}_f\dot{u}+V_t\dot{m}_fu'\\&+V_tm_f'\dot{u}+V_t^2m_f'u'\Big)-(Tu')'\\&=EA_r(v''u'+v'u'')+\frac{1}{2}EA_r\big(3u''u'^2+u''v'^2+2v''v'u'+u''w'^2+2w''w'u'\big)+F_x\end{aligned}\tag{1}$$

$$\begin{aligned}&(m+m_a+m_f)\ddot{v}+c\dot{v}+EIv^{(IV)}+2m_fV_t\dot{v}'+m_fV_t^{2v''}+\Big(\dot{m}_f\dot{v}+V_t\dot{m}_fv'\\&+V_tm_f'\dot{v}+V_t^2m_f'v'\Big)-(Tv')'\\&=EA_rv''+2EA_rv''v'+EA_r(u''u'+v''v'+w''w')+\frac{1}{2}EA_r\big(v''u'^2+2u''u'v'\\&+3v''v'^2+v''w'^2+2w''w'v'\big)+F_y\end{aligned}\tag{2}$$

$$\begin{aligned}&(m+m_a+m_f)\ddot{w}+c\dot{w}+EIw^{(IV)}+2m_fV_t\dot{w}'+m_fV_t^{2w''}+\Big(\dot{m}_f\dot{w}+V_t\dot{m}_fw'\\&+V_tm_f'\dot{w}+V_t^2m_f'w'\Big)-(Tw')'\\&=EA_r(v''w'+v'w'')+\frac{1}{2}EA_r\big(w''u'^2+2u''u'w'+w''v'^2+2v''v'w'+3w''w'^2\big)+F_z\end{aligned}\tag{3}$$

where u, v, and w represent structural displacements in the in-plane (X), axial (Y) and out-of-plane (Z) directions, F_x, F_y, and F_z are the corresponding hydrodynamic forces respectively and V_t is the internal slug translational velocity. The overdot and prime in the equations denote derivatives with respect to time t_i and space y, and T represent tension in space. For risers with varying inclination angles, the change in tension (T) across the length of the cylinder can be expressed as:

$$T=T_0-g\left(m-\frac{\rho\pi D^2}{4}\right)(L-Y)sin\theta\tag{4}$$

Where T_0 is the top pre-tension, g is acceleration due to gravity and L is the total length of the cylinder. The overall structure geometric nonlinearities, mean displacements and 3-D vibrations are accounted for through quadratic and cubic coupling terms in the Eqs. (1-3). The semi-empirical model also takes into account the centrifugal force and the Coriolis force, in addition to inertial and momentum change effects to emulate vibrations due to hydrodynamic slug flows which have been identified as crucial in describing two-phase flow-induced vibrations (Hara, 1973).

2.2. Nonlinear hydrodynamic forces

Vortices are shed when the submerged cylinder oscillates due to internal two-phase slug flows causing hydrodynamic drag and lift forces with frequencies $2\Omega_f$ and Ω_f respectively. The respective drag and lift forces caused by the shed vortices induce oscillations in the in-plane and out-of-plane directions. The oscillations in the in-plane and out-of-plane directions instigate oscillations in the axial direction (Eq. (2)) due to the nonlinear coupling terms in the equations. The fluctuating and self-exciting drag and lift forces can be modelled using the van der Pol wake oscillator equation by introducing wake variables $p=2C_D/Cd_o$ and $q=2C_L/Cl_o$, where C_D, C_L, Cd_o and Cl_o are oscillating drag, oscillating lift, wake associated drag and wake associated lift coefficients respectively (Facchinetti et al., 2004). The wake oscillator model can be expressed as:

$$\ddot{p}+2\varepsilon_u\Omega_f\left(p^2-1\right)\dot{p}+4\Omega_f^2p=\frac{\Lambda_u}{D}\ddot{u}\tag{5}$$

$$\ddot{q}+\varepsilon_w\Omega_f\left(q^2-1\right)\dot{q}+\Omega_f^2q=\frac{\Lambda_w}{D}\ddot{w}\tag{6}$$

Where $\Omega_f=\frac{2\pi S_tV_e}{D}$, S_t is the Strouhal number (assumed to be 0.18 following Song et al. (2011)) and V_e is the external flow velocity. For a stationary cylinder, the drag and lift forces align with in-plane and out-of-plane directions, dictating $F_x=F_D$ and $F_Z=F_L$ whose projection is shown in Fig. 1. During cylinder oscillations, the drag and lift forces become random and no longer correspond to the X and Z direction due to the cylinder relative motion. By following Zanganeh and Srinil (2016), the total and drag and lift forces acting with a clockwise horizontal angle of θ and γ as shown in Fig. 1(c) considering structure and external flow relative velocities, V_{rel} and wake variables, the associated three-dimensional fluid forces can be expressed as:

$$F_x=\frac{1}{4}\rho DV_{rel}C_{l0}q\dot{w}+\frac{1}{4}\rho DV_{rel}C_{d0}p(V-\dot{u})+\frac{1}{2}\rho DV_{rel}\overline{C}_d(V-\dot{u})\tag{7}$$

$$F_y=\frac{1}{4}\rho DV_{rel}C_{l0}q\dot{v}+\frac{1}{4}\rho DV_{rel}C_{d0}p\dot{v}+\frac{1}{2}\rho DV_{rel}\overline{C}_d\dot{v}\tag{8}$$

$$F_z=\frac{1}{4}\rho DV_{rel}C_{l0}q(V-\dot{u})-\frac{1}{4}\rho DV_{rel}C_{d0}p\dot{w}-\frac{1}{2}\rho DV_{rel}\overline{C}_d\dot{w}\tag{9}$$

In which, $V_{rel}=$

$$V_{rel}=\sqrt{(V_e-\dot{u})^2+(\dot{v})^2+(\dot{w})^2}.\tag{10}$$

Where $\overline{C}_d$ is the mean drag coefficient. The corresponding values for C_{d0}, C_{l0}, $\overline{C}_d$, ε_u, ε_w, A_u, A_w are empirical coefficients calibrated by Zanganeh & Srinil (2016) using results from experimental study conducted by Song et al. (2011) are 0.2,0.3 1.2, 0.3,0 0.3, 12 and 12 respectively (Dai et al., 2013). It should be mentioned that the presented model is also capable of predicting vibrations due to external flow (vortex-induced vibrations). However, the focus of this study is to investigate the three-dimensional response of a submerged flexible cylinder subjected to internal two-phase slug flow.

2.3. Dimensionless nonlinear SIV model

Dimensionless terms such as $U=u/D$, $V=v/D$, $W=w/D$, $Y=y/D$, $T_m=\omega_nt_i$, are introduced to the developed equations to achieve better understanding of the model during parametric study. The 3-D dimensionless nonlinear partial differential equations of coupled out-of-plane, in-plane, and axial motions combined with the equation of motion for two-phase internal flow can be expressed as:

$$\begin{aligned}&(1+M)\ddot{U}+2\zeta\dot{U}+E_IU^{(IV)}+2U_rM\dot{U}'+U_r^{2MU''}\\&+\left(\dot{M}\dot{U}+U_r\dot{M}U'+U_rM'\dot{U}+U_r^{2M'}U'\right)-(T_nU')=\frac{E_A}{L_D}(V''U'+V'U'')\\&+\frac{1}{2}\frac{E_A}{L_D}\left(3U''U'^2+U''V'^2+\frac{2}{L_D}V''V'U'+U''W'^2+\frac{2}{L_D}W''W'U'\right)+F_x\end{aligned}\tag{11}$$

$$(1+M)\ddot{V}+2\zeta\dot{V}+E_I V^{(IV)}+2U_r M\dot{V}^{'}+U_r^{2M'}$$
$$+\left(\dot{M}\dot{V}+U_r\dot{M}V^{'}+U_r M^{'}\ddot{V}+U_r^{2M'}W^{'}\right)-(T_n V^{'})^{'}=E_A V^{''}+2\frac{E_A}{L_D}V^{''}V^{'}$$
$$+\frac{E_A}{L_D}(U^{''}U^{'}+V^{''}V^{'}+W^{''}W^{'})$$
$$+\frac{1}{2}\frac{E_A}{L_D}\left(V^{''}U^{'2}+\frac{2}{L_D}U^{''}U^{'}V^{'}+3V^{''}V^{'2}+V^{''}W^{'2}+\frac{2}{L_D}W^{''}W^{'}V^{'}\right)+F_y \tag{12}$$

$$(1+M)\ddot{W}+2\zeta\dot{W}+E_I W^{(IV)}+2U_r M\dot{W}^{'}+U_r^{2MW'}$$
$$+\left(\dot{M}\dot{W}+U_r\dot{M}W^{'}+U_r M^{'}\dot{W}+U_r^{2M'}W^{'}\right)-(T_n W^{'})^{'}$$
$$=\frac{E_A}{L_D}(V^{''}W^{'}+V^{'}W^{''})$$
$$+\frac{1}{2}\frac{E_A}{L_D}\left(W^{''}V^{'2}+W^{''}V^{'2}+\frac{2}{L_D}U^{''}U^{'}W^{'}+\frac{2}{L_D}V^{''}V^{'}W^{'}+3W^{''}W^{'2}\right)+F_z \tag{13}$$

Where, $M=\frac{m_f}{m_0}$, is the dimensionless mass quotient defined as the ratio of internal fluid mass (m_f) to the mass of the cylinder with added mass ($m_0 = m+m_a$), and $L_D=L/D$ is the span ratio. ζ is the damping ratio described as $\frac{1}{m_0\omega_n}c=2\zeta$, where ω_n is the first natural frequency of the cylinder. Bending stiffness of the cylinder E_I in dimensionless form is defined as $E_I=EI\frac{1}{m_0\omega_n^2D^4}$. Likewise, axial stiffness is expressed as the normalized product of modulus of elasticity and cross-sectional area $E_A=\frac{EAr}{m_0\omega_n^2D^2}$. U_r is the dimensionless internal translational velocity expressed as, $U_r=\frac{V_t}{\omega_n D}$. Variation of tension in dimensionless form is expressed as:

$$T_n=T_{n0}-G_n(1+M)(1+Y)sin\theta+G_n\frac{\pi}{4\mu}(1+C_m)(1-Y)sin\theta \tag{14}$$

Where, $T_{n0}=\frac{T}{m_0\omega_n^2D^2}$ and C_m is the added mass coefficient. Non-dimensional tension equation gives rise to a unique parameter $G_n=\frac{g}{w_n^2D}$. Applying dimensionless terms to the wake oscillator model and the three-dimensional hydrodynamic force equations, the corresponding equations become:

$$\frac{d^2p}{dT_m^2}+2\varepsilon_u\Omega(p^2-1)\left(\frac{dp}{dT_m}\right)+4\Omega^2p=A_u\left(\frac{d^2U}{dT_m^2}\right) \tag{15}$$

$$\frac{d^2q}{dT_m^2}+\varepsilon_w\Omega(q^2-1)\left(\frac{dq}{dT_m}\right)+\Omega_f^2q=\Lambda_w\left(\frac{d^2W}{dT_m^2}\right) \tag{16}$$

$$F_x=\frac{1}{4\mu}V_{rel}^{'}C_{l0}q\dot{W}+\frac{1}{4\mu}V_{rel}^{'}C_{d0}p\left(\frac{V_r}{2\pi}-\dot{U}\right)+\frac{1}{2\mu}V_{rel}^{'}\overline{C}_d\left(\frac{V_r}{2\pi}-\dot{U}\right) \tag{17}$$

$$F_y=\frac{1}{4\mu}V_{rel}^{'}C_{l0}q\dot{V}+\frac{1}{4\mu}V_{rel}^{'}C_{d0}p\dot{V}+\frac{1}{2\mu}V_{rel}^{'}\overline{C}_d\dot{V} \tag{18}$$

$$F_z=\frac{1}{4\mu}V_{rel}^{'}C_{l0}q\left(\frac{V_r}{2\pi}-\dot{U}\right)-\frac{1}{4\mu}V_{rel}^{'}C_{d0}p\dot{W}-\frac{1}{2\mu}V_{rel}^{'}\overline{C}_d\dot{W} \tag{19}$$

$$V_{rel}^{'}=\sqrt{\left(\frac{V_r}{2\pi}-\dot{U}\right)^2+(\dot{V})^2+(\dot{W})^2} \tag{20}$$

Where $\mu=\frac{m_0}{\rho_e D^2}$ and ρ_e is the external flow density. $V_{rel}^{'}$ is the dimensionless relative velocity and V_r is the dimensionless external flow velocity. In reality, two-phase flows may develop into different flow patterns in a riser based on the pipe-fluid properties (Bordalo et al., 2008). The flow patterns may be further modified during pipe oscillation. In this study, attention is given to the slug flow regime, assuming that the slug properties analyzed remain undisturbed by pipe oscillations. According to Zhu et al. (2018) slug flow is inherently transient and unsteady. Bowen and Srinil (2020) and several other researchers have suggested that the randomness of slug flow in a flexible cylinder may be approximated by average properties. Therefore, a steady time-varying slug flow is assumed in this study, indicating that the slug sheds liquid from the back at the same rate that the liquid is gathered from the front. This implies that the slug lengths remain constant as each slug unit travels along the pipe. Furthermore, the slug flow is assumed to be fully developed and is modelled as a fluid with time-varying mass using a rectangular pulse train model, implemented with MATLAB codes and functions (Miranda and Paik, 2019). The highly nonlinear partial differential Eqs. (11) – (20) are numerically solved for 3-D dynamic responses of the flexible cylinder by using a finite difference approach in both space and time domain (see Appendix A). Convergence tests of numerical simulations have been performed and the results in Section 3 and 4 are based on the dimensionless time step of 0.001 and 100 spatially discretized elements.

3. Model validation with numerical comparisons

Since experimental studies concerning slug flow induced vibrations of submerged vertical cylinders are sparse, numerical results of the present model is compared with theoretical model results of vertical straight drilling riser by Meng et al. (2018). The drilling riser is a submerged long flexible cylinder with length, $L=500$ m, outer diameter, $D=0.583$ m and inner diameter, $ID=0.489$ m, density $=7850$ kg/m^3, young's modulus, $E=210$ GPa. The density of the surrounding fluid is 1025 kg/m^3. The riser is subjected to internal single-phase flow with a density of 1600 kg/m^3. It should be mentioned that single-phase flows in the model is achieved by considering a constant fluid density along the length of the cylinder.

Fig. 3 displays the comparison between the first six natural frequencies obtained from the present model with results obtained by Meng et al. (2018) for varying flow velocity ranging from 5 to 60 m/s. Free vibration frequency response results are obtained through low amplitude initial condition, allowing the structure to vibrate at its natural frequencies. It can be seen from the Figure that the developed model follows similar trends of reducing natural frequencies as internal flow velocities increase from 5 to 60 m/s. The model is seen to obtain identical natural frequency values at lower flow velocities. However, natural frequency values at higher flow velocities and higher modes (4*th*, 5*th* and 6*th*) are found to be slightly higher than the compared results. Furthermore, an uncertainty analysis is carried out to measure the root mean square errors at each natural frequency. The analysis was conducted by calculating the difference between model and theoretical natural frequency values at each internal flow velocity. The sum of the squared differences is obtained which is then divided by the total number of data points, and the square root of that value gives the root mean square errors (RMSE). The RMSE values for the 1*st*, 2*nd*, 3*rd*, 4*th*, 5*th* and 6*th* natural frequencies were calculated to be 0.038, 0.069, 0.098, 0.138, 0.176 and 0.228, respectively. It could be seen that model predictions of natural frequencies produce low RMSE with errors increasing as the natural frequencies increase. The discrepancies in the predicted natural frequencies and the increasing RSME is due to the fact that the developed model takes into account the geometrical nonlinearities (i.e., spring nonlinear stiffness) as opposed to linear structural equation approach adopted by Meng et al. (2018). Zanganeh and Srinil (2016) previously have observed that models excluding geometric nonlinearities tend to overestimate dominant modes, natural frequencies and in-plane and out-of-plane amplitude results, which is common for a linearized model (Srinil, 2010). The model also captures parametric instabilities at similar flow velocities ($V_t=50$ m/s) for all the 6 modes observed in the literature. It can be seen that the natural frequencies switch to lower frequencies at flow velocities above 50 m/s indicating the existence of parametric instabilities. Overall, it can be concluded that the presented 3-D model provide quantitative similarities when compared with results from previous numerical simulations for submerged vertical flexible risers.

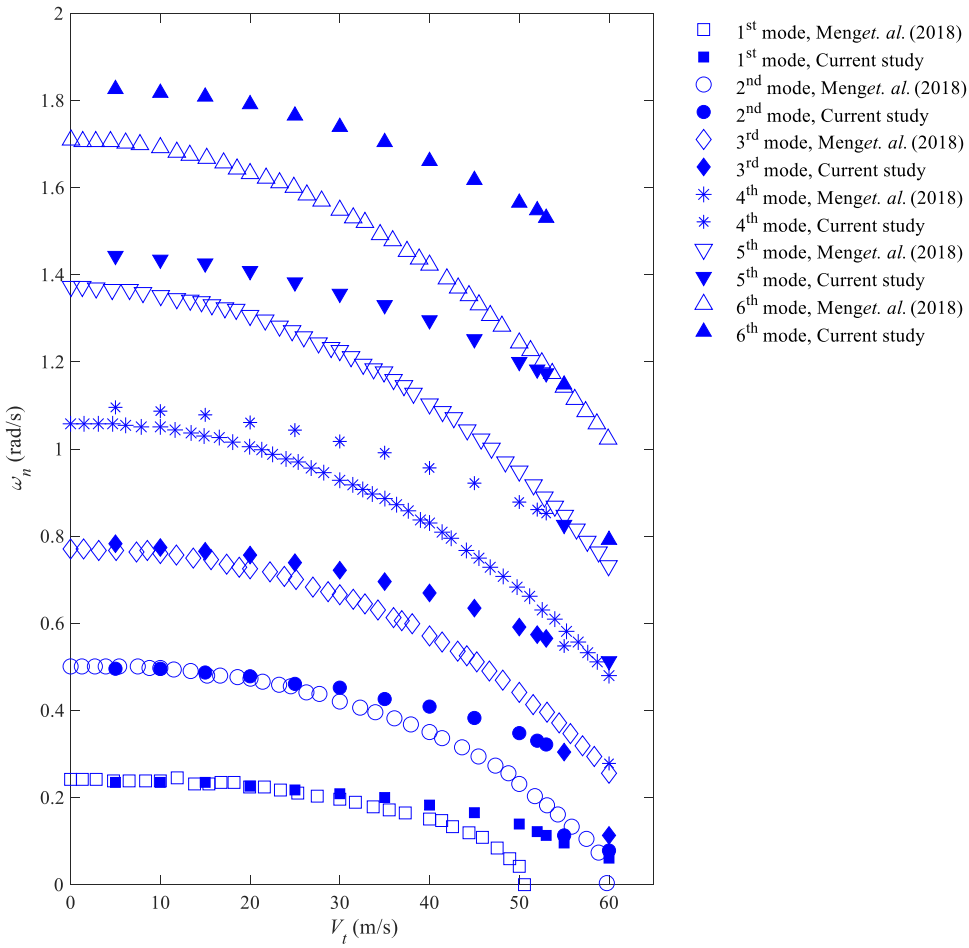

Fig. 3. Comparison between numerical results of obtained natural frequencies for increasing internal flow velocities.

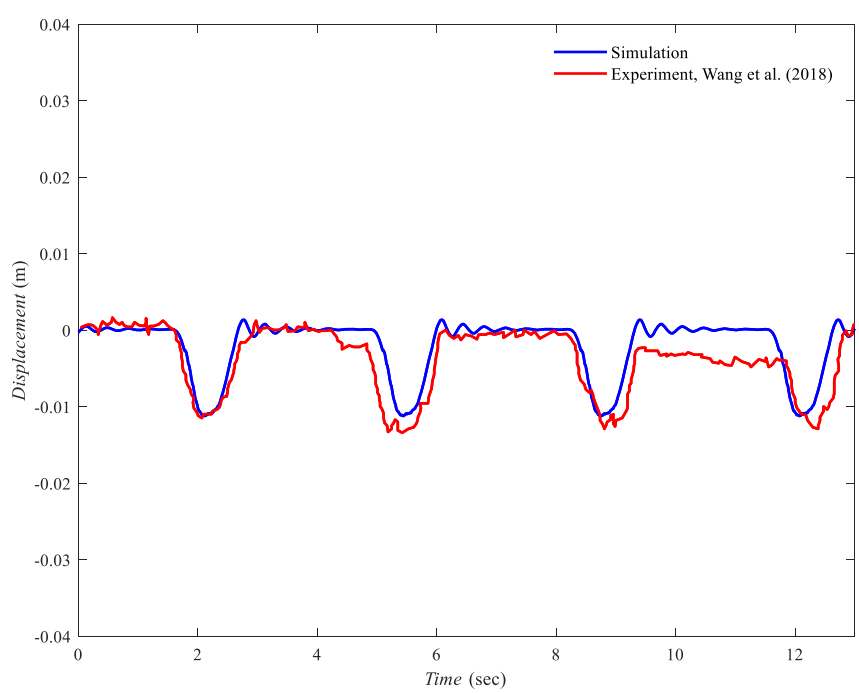

Fig. 4. Time history amplitude comparison between numerical and experimental results (Wang et al. (2018)).

In addition, the developed model has been compared with the experimental tests conducted by Wang et al. (2018) for a horizontal cylinder conveying two-phase slug flows. The fluid-conveying cylinder is surrounded by air with properties $D = 0.063$ m, $L = 3.81$ m, young's modulus, $E = 750$ MPa, density $= 926\text{kg/m}^3$ with internal liquid density $= 1000\text{kg/m}^3$ and viscosity $= 0.001$ Pas. The steady-state internal slug flow is modelled as a rectangular pulse train, where a single slug unit (LU) includes liquid slug (L_S) and an elongated gas bubble over a thin film of liquid (L_F), thin film liquid holdup (H_{LF}), slug liquid holdup (H_{LS}), and translational velocity, (V_t), as shown in Fig. 2. The model follows rectangular waves with flat peaks, where area under the flat peak indicate liquid slug, whose length is L_S. The thin liquid film in the model is represented as the area under the remaining slug unit whose length is L_F. Fig. 4 compares the time history amplitude responses of numerical simulation and experiment results at the midpoint of the cylinder. It is worth mentioning, since the focus of the present comparison is to validate the capabilities of the model in predicting key SIV features, the oscillations in Fig. 4 are depicted around zero and their mean value has been removed. The time-history plot obtained from this study shows that the present model is capable of accurately capturing the SIV out-of-plane amplitude and frequencies compared to the experimental results. The minor discrepancies observed in Fig. 4 are due to differences in slug frequencies between the experiment tests and the simulation. Wang et al. (2018), varied the slug frequencies of each slug unit passing through the cylinder. In their work, the slug length L_S and translational velocity, V_t, for each slug unit vary as 1.19 m, 1.09 m, 0.73 m and 1.19 m and 3.50 m/s, 3.03 m/s, 3.64 m/s and 2.33 m/s, respectively. However, this study employs a steady-state slug flow, where the slug frequencies of all the slug units passing through the cylinder over time remain constant. Therefore, the values for L_S, L_F, and V_t, obtained from the literature, are fixed at 1.19 m, 10.53 m, and 3.5 m/s, respectively, for all the slug units travelling along the cylinder. Secondly, the details of H_{LS} and H_{LF} values are absent in Wang et al. (2018), which may further affect the mean deflection at the cylinder midpoint. In the present study, these key slug flow characteristics were calculated using the *iSLUG* model (Zanganeh et al. (2021)). An uncertainty analysis is performed to measure the error differences between experiment and simulation values. An RSME error of 0.00178 was obtained from calculating the square root of the mean difference in amplitude values at each time step. The low RMSE value, along with the similar trends of amplitude and frequency response observed in Fig. 4, indicates that the model exhibits quantitative similarities when compared with previous experimental results.

4. Numerical results of a long flexible cylinder conveying two-phase slug flows

The long drilling riser used for validation in the previous section is considered for parametric study. The vertical cylinder has an aspect ratio of 858 and is assumed to be submerged in water with no external flow. The effect of the slug flow characteristics mentioned in the previous section, in addition to the mass quotient, M, which is the ratio of internal fluid mass over the mass of empty pipe with added mass, on the dynamic response of the vertical riser, is investigated in this section. In addition, four dimensionless translation velocities ($U_r = 47.3$, 94.6,141.8 and 189.1) is considered for each varying slug parameter to capture maximum features of slug flow induced vibrations.

Table 1 presents the details of all the slug characteristics that are varied for the parametric study. Four cases for each slug property are considered at four different translational velocities. A total of 16 cases are considered to anlayze the effect of one slug property. The slug liquid holdup (H_{LS}), and the thin liquid film holdup (H_{LF}), are varied in fractions of 15 from 0 to 1. Where the value 0 denotes empty pipe and 1 indicate completely-filled liquid slug holdup (H_{LS}) and thin film holdup (H_{LF}) respectively. When varying H_{LS}, H_{LF} is considered to be 0 for all 16 cases and while varying H_{LF}, the H_{LS} parameter is considered be 1. The slug liquid length, L_S, is varied as a function of a constant slug unit length L_U (17D) where 0.1, 0.35, 0.6 and 0.85 represent percentages of L_U. The L_U parameter is varied as a function cylinder diameter from 5D to 40D, during which L_S and L_F are divided into equal halves for every case of L_U considered. Similarly, the mass quotient cases are varied as half, two and four times the fluid density considered during validation, while L_S and L_F values correspond to the highest amplitude observed during the L_S case study. For all the cases of L_S, L_U and M the H_{LS} and H_{LF} values are 1 and 0 respectively to capture maximum momentum exchange between the two phases.

Table 1
Slug flow properties considered in cases of varying (a) H_{LS} (b) H_{LF} (c) L_S (d) L_U (e) M.

(a)

U_r	H_{LS}	H_{LF}	L_S/D	L_F/D	L_U	M
47.3, 94.6, 141.8, 189.1	0.55	0	16	14	30D	1.788
	0.7	0	16	14	30D	1.788
	0.85	0	16	14	30D	1.788
	1	0	16	14	30D	1.788

(b)

U_r	H_{LF}	H_{LS}	L_S/D	L_F/D	L_U	M
47.3, 94.6, 141.8, 189.1	0	1	16	14	30D	1.788
	0.15	1	16	14	30D	1.788
	0.3	1	16	14	30D	1.788
	0.45	1	16	14	30D	1.788

(c)

U_r	L_S/D	H_{LS}	H_{LF}	L_F/D	L_U	M
47.3, 94.6, 141.8, 189.1	0.1	1	0	0.9	30D	1.788
	0.35	1	0	0.65	30D	1.788
	0.6	1	0	0.4	30D	1.788
	0.85	1	0	0.15	30D	1.788

(d)

U_r	L_U	H_{LS}	H_{LF}	L_S/D	L_F/D	M
47.3, 94.6, 141.8, 189.1	5D	1	0	0.5	0.5	1.788
	10D	1	0	0.5	0.5	1.788
	20D	1	0	0.5	0.5	1.788
	40D	1	0	0.5	0.5	1.788

(e)

U_r	M	H_{LS}	H_{LF}	L_S/D	L_F/D	L_U
47.3, 94.6, 141.8, 189.1	0.894	1	0	0.35	0.65	30D
	1.788	1	0	0.35	0.65	30D
	3.576	1	0	0.35	0.65	30D
	7.151	1	0	0.35	0.65	30D

4.1. Slug flow induced amplitude response and mean displacements

Fig. 5(a-d) and (e-h) displays out-of-plane and in-plane maximum RMS amplitude response of the riser for all the slug flow parameters considered. While varying H_{LS} (Table 1(a)), it was observed that at low internal flow velocities ($U_r = 47.3$ and 94.6), the maximum RMS amplitude increased linearly with each increase in the slug holdup value, H_{LS} as seen in Fig. 5(a) and (e). The maximum amplitude increases up to four times in the out-of-plane direction and up to eight times in the in-plane direction when $H_{LS} = 1$ (completely-filled), compared to when $H_{LS} = 0.55$ (half-filled). At higher translational flow

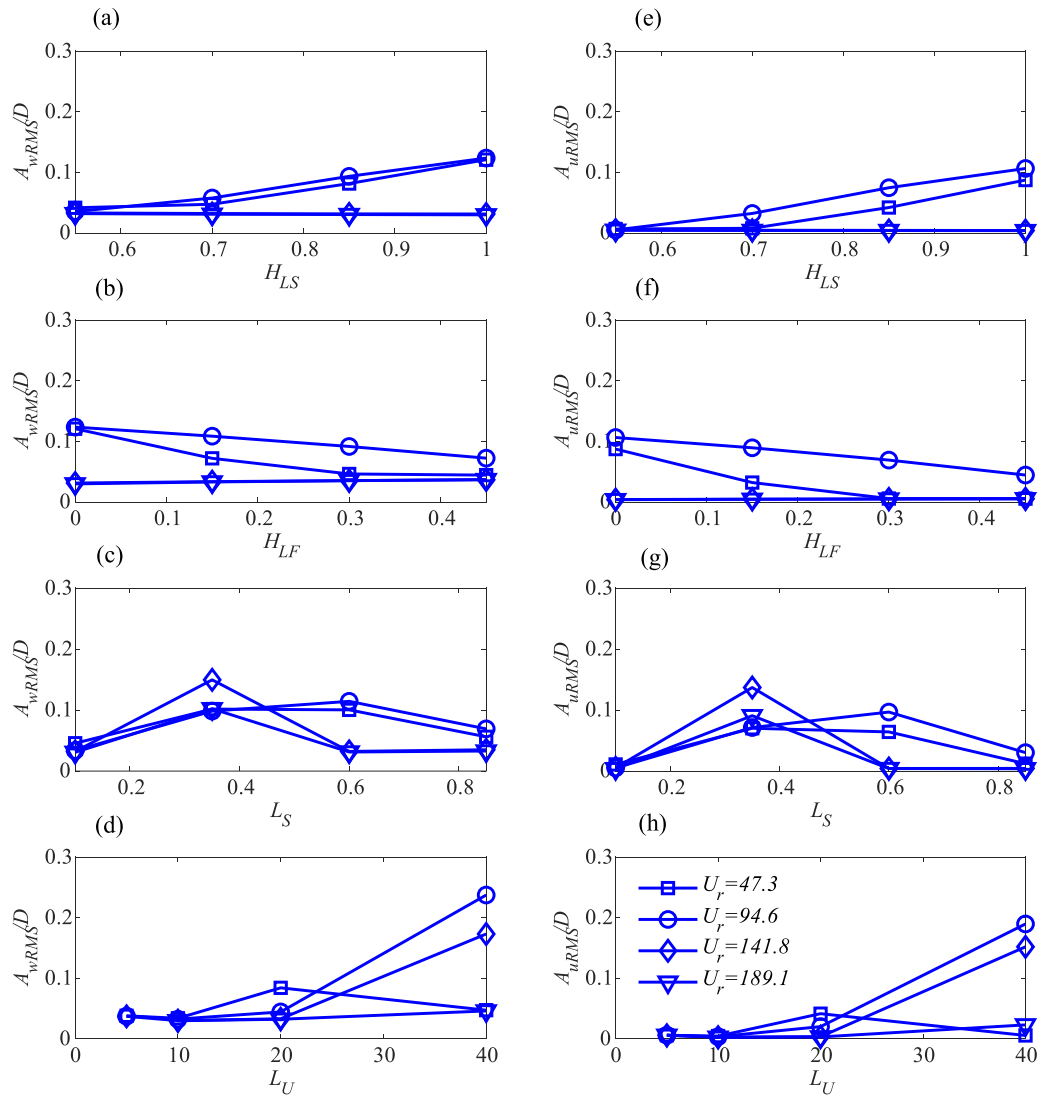

Fig. 5. Comparison of maximum (a-d) out-of-plane and (e-h) in-plane RMS amplitudes for varying (a-e) H_{LS}, (b-f) H_{LF}, (c-g) L_S, (d-h) L_U.

velocities ($U_r = 141.8$ and 189.1), vibration amplitudes are significantly lower, and no changes in amplitude are observed as H_{Ls} increases. This may be due to the fact that at higher flow velocities, the slug travels through the pipe much faster, leaving very little time for the fluid to exert forces on the structure, thereby making it insignificant. This feature has also been previously observed by Bowen and Srinil (2020) for catenary pipes conveying two-phase slug flows. At lower flow velocities, the increase in amplitude with increase in H_{LS} may be attributed to the overall increase in the mass of the cylinder, allowing for greater mass and momentum fluctuations over time.

In the case of varying H_{LF} (Table 1(b)), at lower flow velocities, the maximum amplitude decreases with an increase in H_{LF} as seen in Fig. 5 (b) and (f). This decrease is expected as the interaction between the liquid and gas phases becomes minimal, resulting in lower overall fluctuations of the two-phase flow. At higher flow velocities, the maximum amplitude trends are similar to those previously discussed for H_{LS}, with negligible changes in amplitude.

Furthermore, in the case of varying L_S (Table 1(c)), the out-of-plane and in-plane RMS amplitudes are found to be the highest when L_S is approximately half of L_U for all four flow velocities considered. It can be observed from Fig. 5(c) and (g) that the maximum amplitude increases with an increase in L_S and then decreases significantly when L_S is almost the same length as L_U. As mentioned earlier, this can be attributed to the minimal interaction between the two phases when L_S is close to zero or almost equal to L_U, resulting in inadequate mass and momentum fluctuations.

However, as the length of one slug unit L_U increases (Table 1(d)), the maximum amplitude remains low and constant for the first three cases and then increases for the fourth case in which L_U is the largest. For flow velocities 94.6, 141.8, and 189.1, the maximum amplitude is observed at $L_U = 40$D as seen in Fig. 5(d) and (h). Highest amplitude response during the accumulation of the longest liquid slug has been previously observed by Miranda and Paik (2019) and Wang et al. (2018). During the lowest flow velocity case, $U_r = 47.3$, the maximum amplitude is observed at $L_U = 20$D, which is half the maximum amplitude observed when $L_U = 40$D (longest liquid slug).

The highest amplitude response among all the slug properties considered in this study is observed when the mass quotient, M, (Table 1

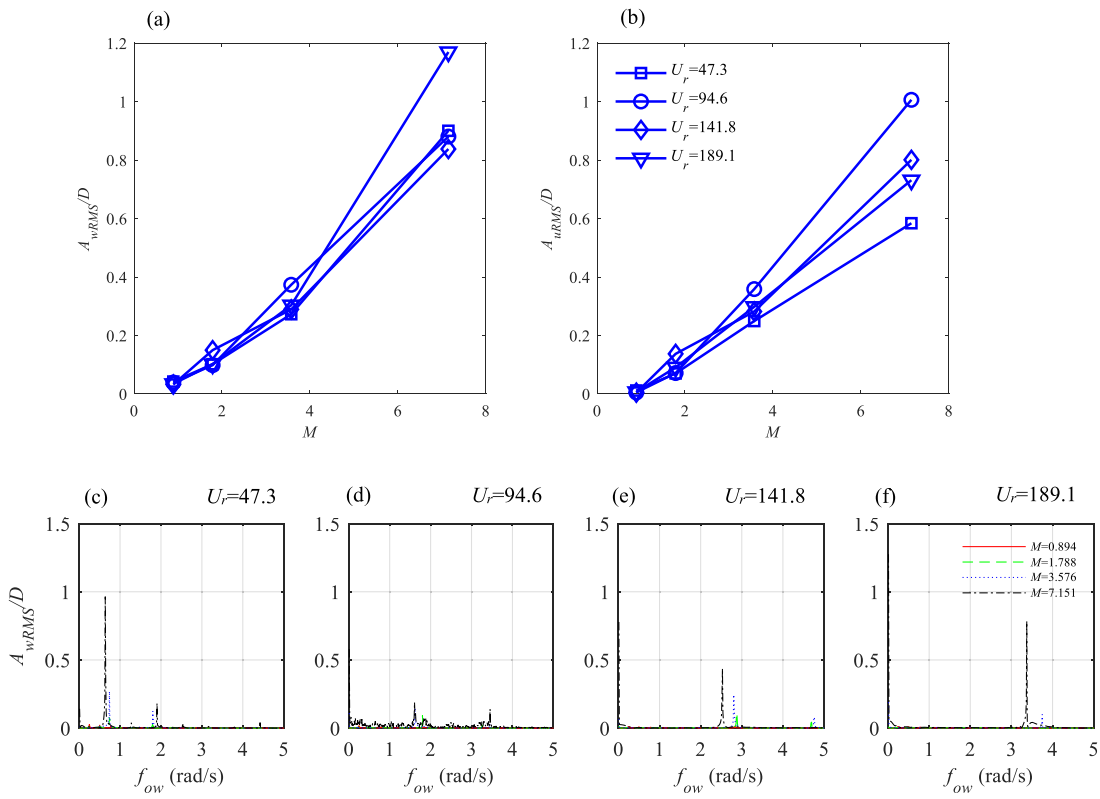

Fig. 6. Maximum (a) out-of-plane and (b) in-plane RMS amplitudes and (c-f) frequency response plots for cases of varying mass quotient (*M*).

(e)) is three times the mass quotient previously considered, as seen in Fig. 6(a) and (b). The RMS amplitude is observed to linearly increase with every increase in the mass quotient parameter. The highest amplitude observed is almost 50 times higher (0.03 to 1.6 in the out-of-plane direction and 0.018 to 1.4 in the in-plane direction) than the maximum amplitude noticed during the lowest mass quotient case. This increase can be attributed to the significant increase in fluid density, which leads to increased mass-momentum fluctuations in the two-phase slug flow and internal forces on the riser.

In addition, at high mass quotient cases ($M = 3.58$ and 7.15) during internal flow velocities $U_r = 94.6$, 141.8, and 189.1, the riser is observed to experience mean displacements in both the out-of-plane and in-plane directions, as shown in Fig. 7(b-d) and (f-h) respectively. The riser drifts from its original *XY* position and reaches a high amplitude steady-state oscillation from the attained curved configuration in both directions. This can be observed in the colour bars associated with Figs. 7(a-d) and (e-h). This mean drift can be a consequence of slug-induced high amplitude oscillations, which lead to disturbances in the external fluid surrounding the riser. These disturbances create oscillating drag and lift forces on the pipe due to the nonlinear external fluid forcing terms in the developed model (Zanganeh and Srinil, 2016).

Among all the slug flow properties considered amplitude-modulation responses are observed when the riser is exposed to the longest slug unit at $L_U = 40$D and $U_r = 94.6$, 141.8, and 189.1, respectively, as shown in Fig. 8(a) and (b). This phenomenon occurs when multiple dominant frequencies of vibration occur over time, as previously observed by Zhu et al. (2018b) during an experimental study of slug-induced oscillations of long catenary pipes and Meng et al. (2020) for flexible marine risers subjected to simultaneous VIV and internal slug flow forces. Such amplitude-modulation response can lead to severe fatigue damage and should be considered during the life cycle analysis of pipelines conveying two-phase slug flows at higher L_U values.

Furthermore, comparison of maximum amplitudes obtained during single and two-phase slug flows for varying internal flow velocities are shown in Fig. 8(c) and (d). It can be observed that the maximum amplitude obtained for two-phase slug flows at lower flow velocities $U_r = 47.3$ and 94.6 is significantly higher than the maximum amplitudes obtained for single-phase flow during similar flow velocities. However, at higher flow velocities ($U_r = 141.8$, 189.1), the maximum amplitudes are found to be closer to each other. It should also be mentioned that for all the cases considered in this study, an initial condition was introduced to the riser such that the cylinder oscillates freely (self-excited without time-dependent force) in the out-of-plane direction only. However, simultaneous out-of-plane and in-plane oscillations are observed as seen in Fig. 8(a-b), where oscillations in the in-plane direction, except for high mass quotient cases, starts several seconds after the riser begins to oscillate in the out-of-plane direction. This occurrence is attributed to the nonlinear couplings present in the developed equations, resulting from the consideration of geometric and hydrodynamic nonlinearities.

4.2. Slug flow induced oscillation frequencies

Frequency domain analysis of the above-mentioned riser displacements due to variations in slug flow characteristics is carried out using the fast Fourier transform (*FFT*) approach and depicted in Fig. 9(a-p). It is observed that the natural frequencies of the first six excited modes, except in the cases of varying mass quotient, remain unchanged during two-phase slug flow when compared to the natural frequencies obtained during single-phase flow for all four internal flow velocities considered.

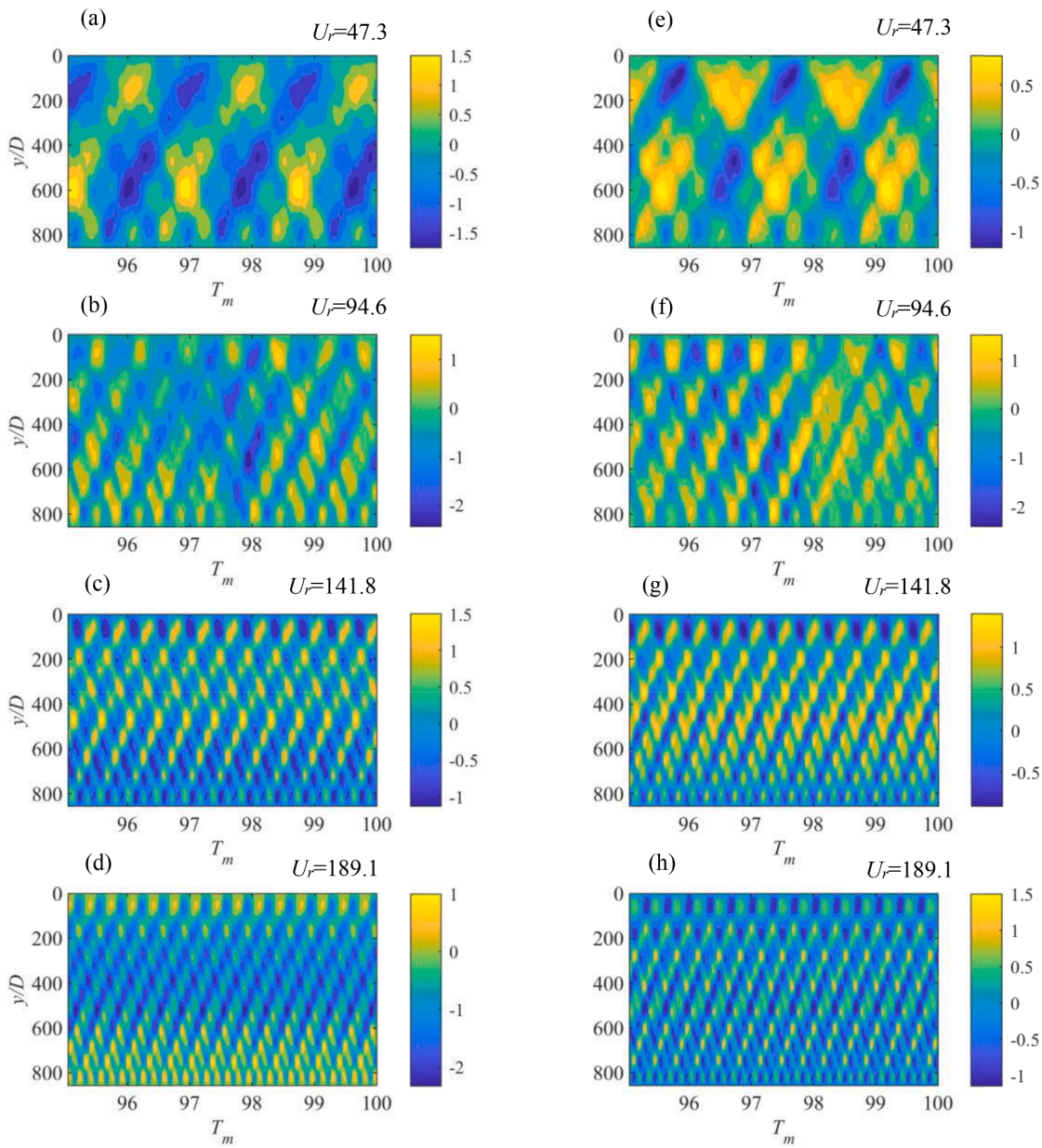

Fig. 7. Space time varying (a-d) out-of-plane and (e-h) in-plane responses of the cylinder experiencing mean drifts during the highest mass quotient case (M =7.15).

The oscillation frequencies, f_0, shown in Fig. 9 can be associated with the natural frequencies shown in Fig. 3 to obtain dominant oscillation frequencies during each case considered in the parametric study. The results of the frequency domain analysis indicate that, although the obtained natural frequencies remain consistent during the parametric study for all six modes, the dominant modes and their corresponding dominant oscillation frequencies vary when the slug flow characteristics are altered.

Fig. 9(a-p) illustrates frequency analysis of out-of-plane riser displacements using *FFT*. The Figure describes oscillation frequency, f_0, *vs* amplitude plots at varying internal flow velocities. It was observed that the oscillation frequencies in the in-plane direction were the same as the frequencies in the out-of-plane direction and hence, Fig. 9 plots show oscillation frequencies in the out-of-plane direction. The dominant modes and their corresponding frequencies are found to switch to higher modes and frequencies when the riser experiences high amplitudes of oscillations at specific slug formations. In cases where the amplitude initially increases and then decreases or vice versa, such as H_{LS}, L_S, and L_U cases, the dominant mode and frequency follow the same trend as the oscillation amplitudes as seen in Fig. 9. When there is minimum or no change in the oscillation amplitudes, for example, H_{LF} cases, the dominant oscillation frequency and mode also remain constant.

It should also be mentioned that the same trends can be observed for every increase in the internal flow velocity. For the mass quotient (M) cases, Fig. 6(c-f), it can be observed that the dominant mode transitions to a lower mode when the amplitude increases with an increase in the mass quotient value for all four internal flow velocities considered. Similarly, the excited oscillation frequencies are seen to decrease as the

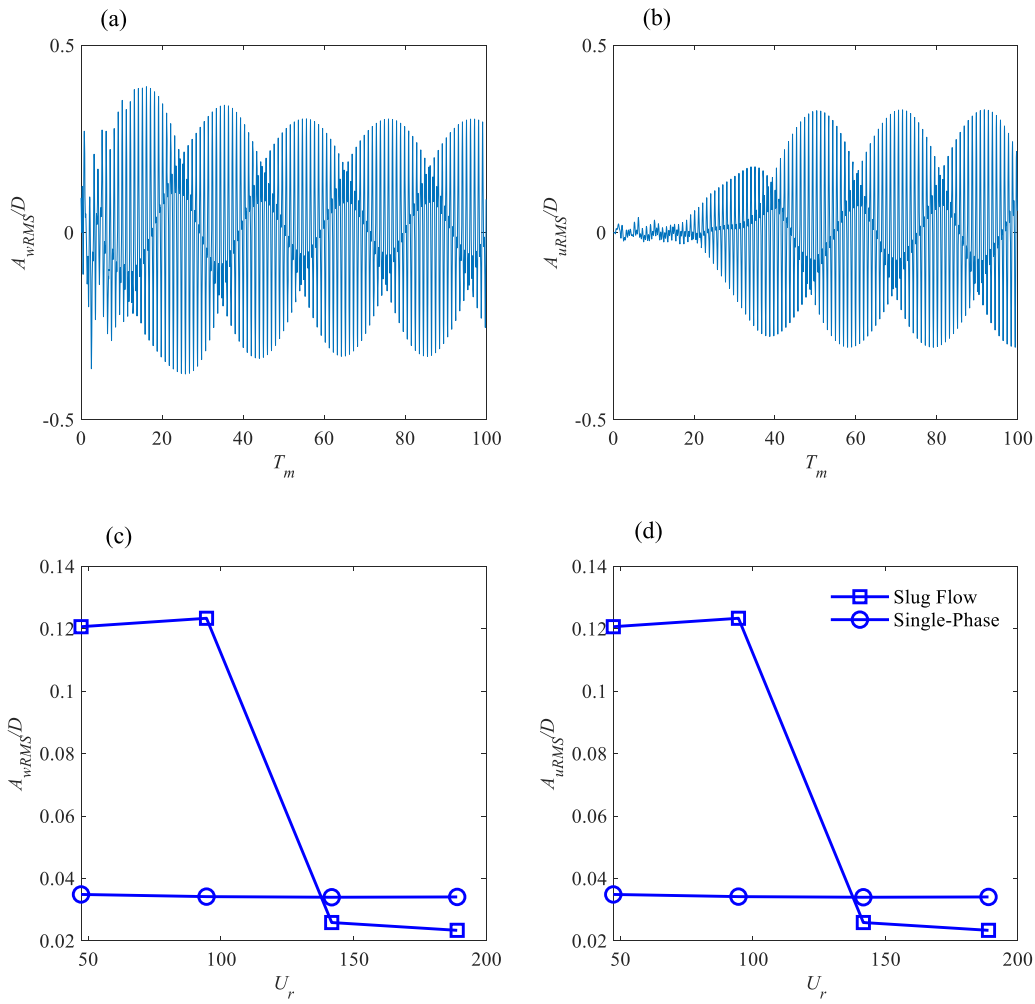

Fig. 8. (a) Out-of-plane and (b) in-plane time history amplitude-modulation response for $L_U = 40D$ at $U_r = 94.6$ and comparison of maximum (c) out-of-plane and (d) in-plane amplitudes of two-phase slug flows and single-phase flows at varying internal velocities.

mass quotient value increases. This decrease in frequency is expected and has been observed in previous studies related to internal flow-induced vibration due to the effect of increased overall mass of the riser in high mass quotient cases. Additionally, it should be noted that the mode switching phenomenon over time does not occur for all the cases considered in this study. Overall, the results of the frequency domain and modal analysis show that the dominant modes and frequencies alter when the considered slug flow properties are varied at different flow velocities.

4.3. Axial oscillation responses and large amplitude scenarios

In addition to the two-dimensional out-of-plane and in-plane oscillations observed in the previous sections, pipe oscillations in the axial direction and mean displacements could be noticed at high mass quotient cases ($M = 3.576, 7.151$) for all the internal flow velocities considered, as shown in Fig. 10 (a-d). However, the oscillation amplitudes in the axial direction are observed to be low but considerable when compared to the out-of-plane and in-plane amplitudes. It should also be mentioned that mean displacements during oscillations in the axial direction could also be observed from the colour bars in Fig. 10(a-d). The oscillations in the axial direction at high mass quotient can be attributed to the effect of mean displacements and high oscillation amplitudes in both the out-of-plane and in-plane directions, leading to hydrodynamic forces in the axial direction and three-dimensional (out-of-plane, in-plane and axial) oscillations arising from nonlinear couplings present in the equation. The effect of axial oscillations due to mean drag amplifications and high oscillation amplitudes has been previously observed by Zanganeh and Srinil (2016) for flexible oscillating cylinders experiencing vortex-induced vibrations.

Furthermore, it can be observed from the previous sections that oscillation amplitudes of the cylinder and the corresponding frequency and dominant modes increase with increase in smaller velocities ($U_r = 47.3, 94.6$) and decrease at higher flow velocities ($U_r = 141.8, 189.1$) for H_{LS}, H_{LF} and L_S study cases. For L_U and mass quotient, M, cases, it is vice-versa, where $U_r = 94.6$ is observed to be the flow velocity experiencing highest vibration response among all the flow velocities considered. A noticeable aspect of the presented model apart from three-dimensional oscillations and the consideration of geometric and hydrodynamic nonlinearities is the low computational effort required to perform each simulation. Simulations with reliable results of oscillation amplitudes, frequencies and mode numbers of each case discussed in this study could be completed within 48 h.

A new non-dimensional parameter, similar to the Strouhal number, is introduced to predict high oscillation amplitudes scenarios. This parameter is derived based on the results obtained from the parametric study conducted in this paper. The maximum RMS amplitude responses in the out-of-plane, in-plane and axial direction is compared using the dimensionless parameter described as:

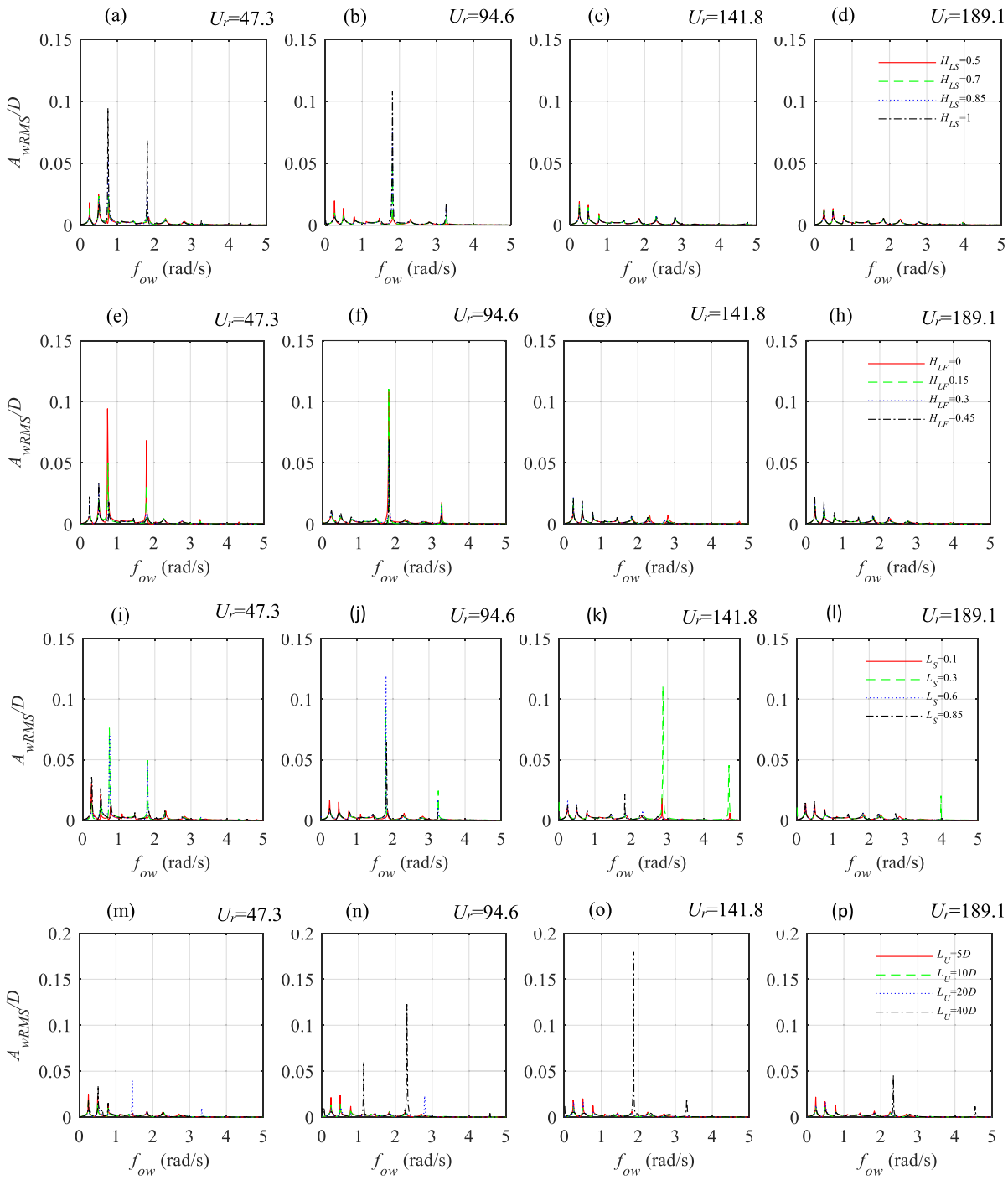

Fig. 9. Out-of-plane frequency response plots of varying internal slug characteristics, (a-d) H_{LS} (e-h) H_{LF} (i-l) L_S (m-p) L_U at increasing internal flow velocities.

$$U_r^{'} = \frac{V_t}{F_{DM}\ D}$$

Where, F_{DM} is the frequency of the dominant mode resulting from each case and D is the outer diameter of the cylinder. Fig. 11(a-b) displays the maximum RMS out-of-plane and in-plane amplitude and its associated $U_r^{'}$ obtained for all the 80 cases considered for parametric study. Results of this comparison reveal that high maximum RMS amplitudes due to internal two-phase slug flow occur between the $U_r^{'}$ range of 2 - 18. It can be inferred from Fig. 11 that all $U_r^{'}$ cases outside this range produce low amplitude oscillations. This inference is plausible because, as observed in the previous sections for cases experiencing high amplitude oscillations, the corresponding dominating mode and frequency of the cylinder are also noticeably high. To verify this finding one case of $U_r^{'}$ outside the mentioned range and one case within the high amplitude range were examined. The F_{DM} were arbitrarily chosen and its equivalent translational velocity was calculated. The slug properties for these cases were chosen based on previous high amplitude response parameters as shown in Table 2. Results from the simulation show similar trends of high RMS amplitude response for case 1 where $U_r^{'}$ is within the high amplitude range and similarly case 2 show low RMS amplitude response in both out-of-plane and in-plane directions as shown in Figs. 11(a) and (b).

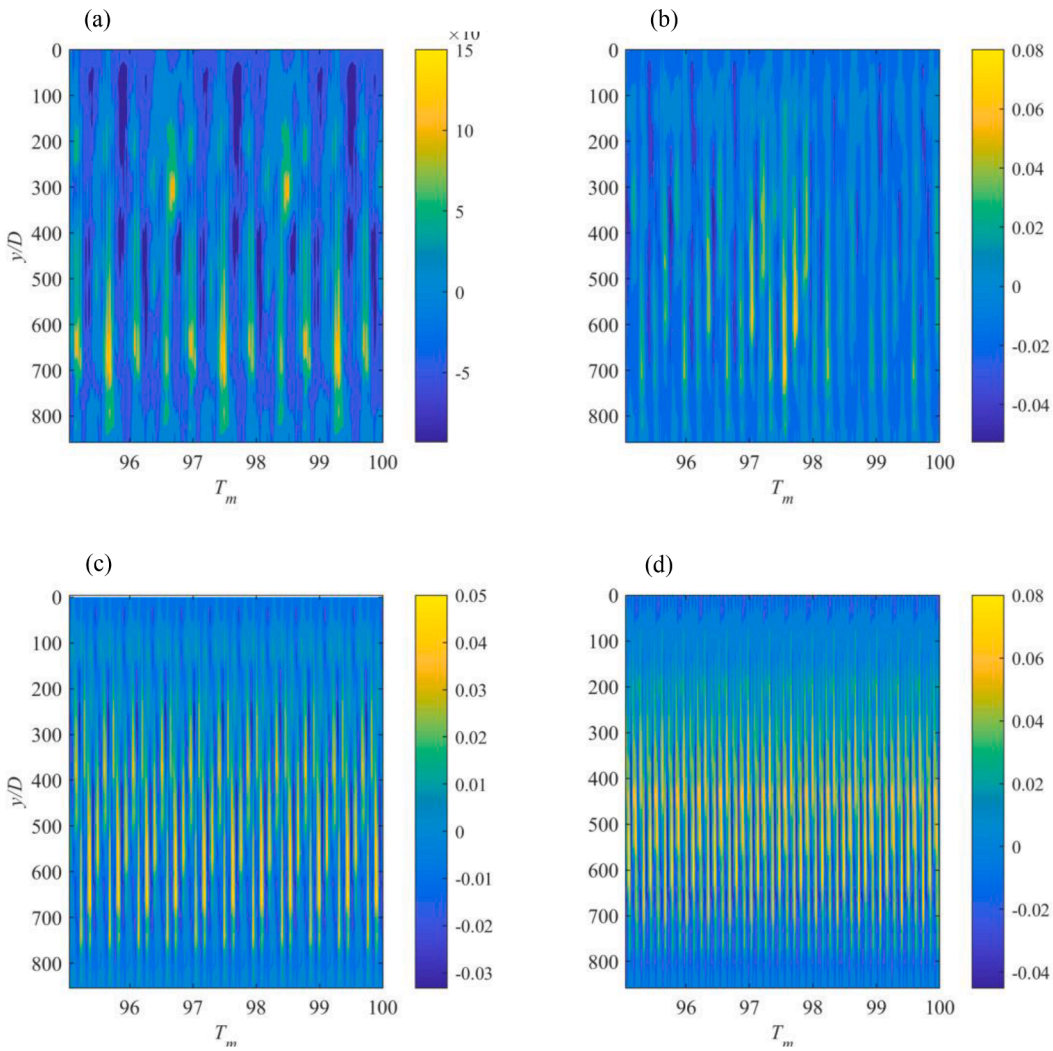

Fig. 10. Space time varying displacements in the axial direction at mass quotient, $M = 7.151$ and varying internal flow velocities. (a) $U_r = 47.3$ (b) $U_r = 9\ 4.6$ (c) $U_r = 141.8$ (d) $U_r = 189.1$.

5. Conclusions

A three-dimensional phenomenological model for the analysis and prediction of coupled out-of-plane, in-plane and axial slug flow induced vibrations of a long flexible cylinder is presented in this study. The developed model accounts for both geometric and hydrodynamic nonlinearities and is capable of capturing mass variations in the slug flow regime. Through cubic and quadratic nonlinear terms, the model is coupled with equations involving centrifugal and Coriolis force for the prediction of two-phase SIV. The model combines external nonlinear fluid forcing terms through oscillatory lift and drag forces. In this study, particular attention is given to the slug flow regime. Hence, the model employs an idealized slug flow concept represented by a rectangular pulse train model, assuming that slug flow properties are fully developed and unaffected by pipe oscillations. A space-time finite difference approach has been used to conduct numerical integrations of highly nonlinear partial differential equations present in the model. Parametric study explores the effects of key slug characteristics and provides insights into several SIV nonlinear dynamic phenomena dictating the response of a long flexible cylinder. The key features are summarized as follows.

- The slug flow induced RMS amplitudes are observed to increase at lower slug translational velocities and decrease at higher translational velocities.
- Simultaneous three-dimensional out-of-plane, in-plane and axial oscillations are observed due to nonlinear coupling terms in the presented model.
- The longest slug unit generate large amplitude-modulation response which can lead to increased fatigue damages over time.
- Mean displacements due to high internal fluid density and large amplitude response in the out-of-plane and in-plane directions induces external hydrodynamic forces on the cylinder leading to oscillations in axial direction because of nonlinear couplings.
- Changes in the two-phase slug flow oscillation frequencies were found to be negligible when compared to the single-phase oscillation frequencies for all the internal translational velocities considered. However, the dominant modes and oscillation frequencies vary according to distinct slug formations and are found to exhibit a linear relationship with the overall amplitude response.
- A dimensionless parameter $U_r^{'}$ is introduced for the purpose of predicting high oscillation amplitude scenarios corresponding to the cases considered in this study. $U_r^{'}$ values ranging from 2 to 18 were found to generate high amplitude responses while the other values outside this range generate low oscillation amplitudes.

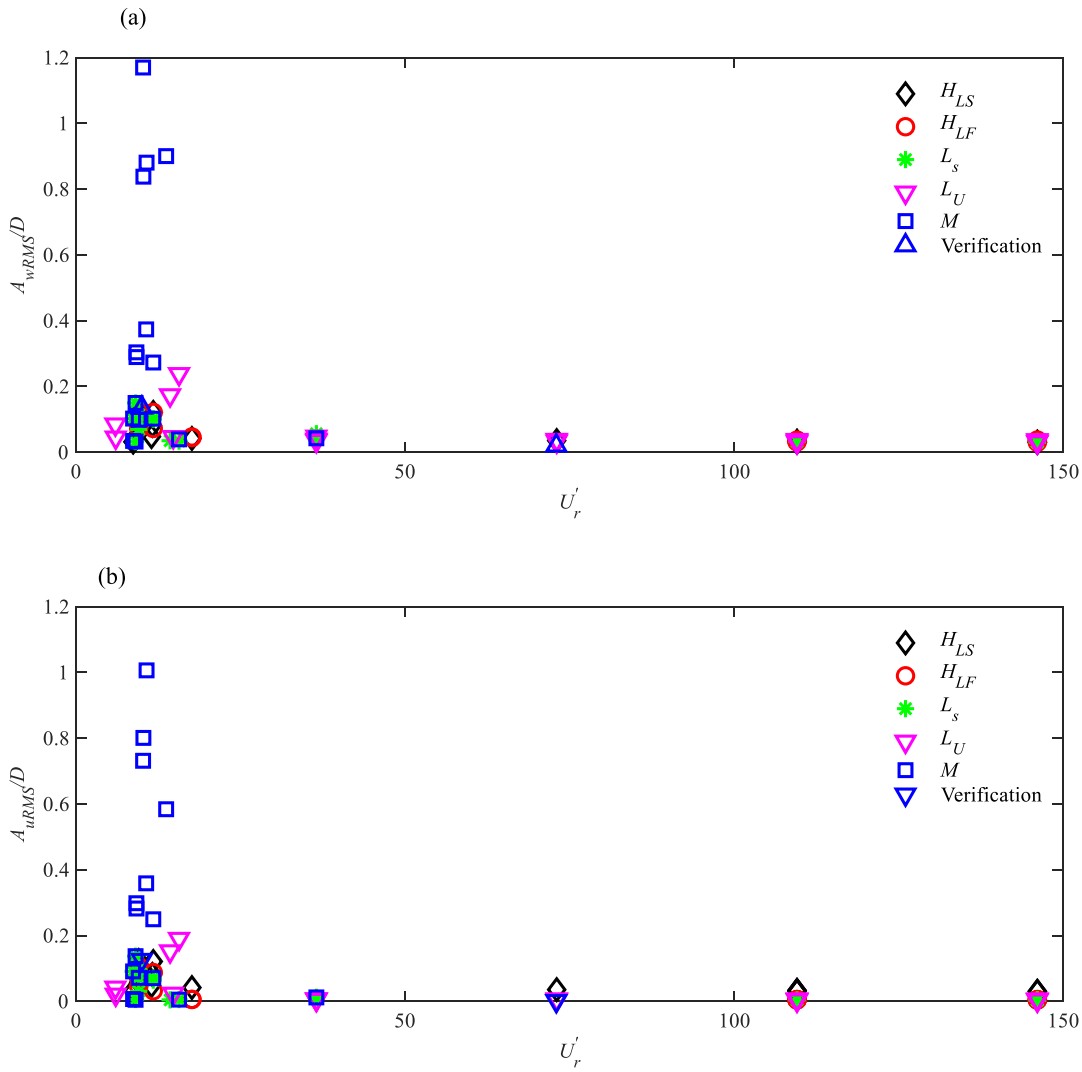

Fig. 11. Comparison of maximum RMS (a) out-of-plane and (b) in-plane amplitude response of all the cases considered for parametric study using new dimensionless parameter U_r'.

Table 2
Specified slug flow parameters for verification.

	Dominant Mode	F_{DM}	H_{LS}	H_{LF}	L_S	L_F	M	D	U_r
10	1	0.235	1	0	6.1	11.4	1.788	0.583	94.46
73	3	0.730	1	0	6.1	11.4	1.788	0.583	293.98

Model validations are performed through comparisons with published numerical and experimental results. Results exhibit quantitative similarities in amplitude and frequency response with minor discrepancies, attributed to the consideration of a more inclusive model that takes into account the structural and geometric nonlinearities. Future studies can explore the three-dimensional fluid-structure interaction phenomena of horizontal flexible cylinders subjected two-phase slug flows, as well as the combined effects of forces arising from two-phase slug flows and vortex-induced vibrations.

CRediT authorship contribution statement

Hareesh Narain Ravindran Meenakumari: Writing – original draft, Validation, Methodology, Investigation, Conceptualization. **Hossein Zanganeh:** Writing – review & editing, Supervision. **Mamdud Hossain:** Writing – review & editing, Supervision.

Declaration of competing interest

The authors declare that they have no known competing financial interests or personal relationships that could have appeared to influence the work reported in this paper.

Data availability

Data will be made available on request.

Appendix A. Finite Difference Scheme

The nonlinear dimensionless Eqs. (11)–(20) were discretized using a standard finite difference scheme of the second order in both space and time domains following Gao et al. (2019). The total time t_{total}, and the cylinder span ratio (L_D) were subdivided into n and i segments, respectively, such that each time step can be obtained as $\Delta T_m = t_{total}/n$ and each space elements can be obtained as $\Delta Y = L/\ (D \times i)$. The distinct space locations and time were expressed as $Y = Y_i$ and $T_m = T_{mn}$ where $i = 0, 1, 2, 3\ldots.., i_{end}$ and $n = 0, 1, 2, 3, \ldots\ldots., n_{end}$. The dimensionless parameters U, V, W, p, and q at location Y_i with time T_{mn} are depicted as U_n^i, V_n^i, W_n^i, p_n^i, and q_n^i respectively. The resulting finite difference derivatives with respect to U, V, W, p and q are expressed as:

$$\frac{\partial^2 U}{\partial T_m^2} = \frac{U_{n-1}^i - 2U_n^i + U_{n+1}^i}{\Delta T_m^2}$$

$$\frac{\partial U}{\partial T_m} = \frac{U_{n+1}^i - U_{n-1}^i}{2\Delta T_m}$$

$$\frac{\partial U}{\partial Y} = \frac{U_{n+1}^{i+1} - U_{n+1}^{i-1}}{2\Delta Y}$$

$$\frac{\partial^2 U}{\partial Y^2} = \frac{U_{n+1}^{i+1} - 2U_{n+1}^i + U_{n+1}^{i-1}}{\Delta Y^2}$$

$$\frac{\partial^4 U}{\partial Y^4} = \frac{6U_{n+1}^i - 4U_{n+1}^{i+1} + U_{n+1}^{i+2} - 4U_{n+1}^{i-1} + U_{n+1}^{i-2}}{\Delta Y^4}$$

$$\frac{\partial^2 U}{\partial Y \partial T_m} = \frac{U_{n+1}^{i+1} - U_{n+1}^{i-1} - U_{n-1}^{i+1} + U_{n-1}^{i-1}}{4\Delta T_m \Delta Y}$$

$$\frac{\partial^2 V}{\partial T_m^2} = \frac{V_{n-1}^i - 2V_n^i + V_{n+1}^i}{\Delta T_m^2}$$

$$\frac{\partial V}{\partial T_m} = \frac{V_{n+1}^i - V_{n-1}^i}{2\Delta T_m}$$

$$\frac{\partial V}{\partial Y} = \frac{V_{n+1}^{i+1} - V_{n+1}^{i-1}}{2\Delta Y}$$

$$\frac{\partial^2 V}{\partial Y^2} = \frac{V_{n+1}^{i+1} - 2V_{n+1}^i + V_{n+1}^{i-1}}{\Delta Y^2}$$

$$\frac{d^4 V}{\partial Y^4} = \frac{6V_{n+1}^i - 4V_{n+1}^{i+1} + V_{n+1}^{i+2} - 4V_{n+1}^{i-1} + V_{n+1}^{i-2}}{\Delta Y^4}$$

$$\frac{\partial^2 V}{\partial Y \partial T_m} = \frac{UV_{n+1}^{i+1} - V_{n+1}^{i-1} - V_{n-1}^{i+1} + V_{n-1}^{i-1}}{4\Delta T_m \Delta Y}$$

$$\frac{\partial^2 W}{\partial T_m^2} = \frac{W_{n-1}^i - 2W_n^i + W_{n+1}^i}{\Delta T_m^2}$$

$$\frac{\partial W}{\partial T_m} = \frac{W_{n+1}^i - W_{n-1}^i}{2\Delta T_m}$$

$$\frac{\partial W}{\partial Y} = \frac{W_{n+1}^{i+1} - W_{n+1}^{i-1}}{2\Delta Y}$$

$$\frac{\partial^2 W}{\partial Y^2} = \frac{W_{n+1}^{i+1} - 2W_{n+1}^i + W_{n+1}^{i-1}}{\Delta Y^2}$$

$$\frac{\partial^4 W}{\partial Y^4} = \frac{6W_{n+1}^i - 4W_{n+1}^{i+1} + W_{n+1}^{i+2} - 4W_{n+1}^{i-1} + W_{n+1}^{i-2}}{\Delta Y^4}$$

$$\frac{\partial^2 W}{\partial Y \partial T_m} = \frac{W_{n+1}^{i+1} - W_{n+1}^{i-1} - W_{n-1}^{i+1} + W_{n-1}^{i-1}}{4\Delta T_m \Delta Y}$$

$$\frac{\partial^2 q}{\partial T_m^2} = \frac{q_{n-1}^i - 2q_n^i + q_{n+1}^i}{\Delta T_m^2} \quad \frac{\partial q}{\partial T_m} = \frac{q_{n-1}^i - q_{n+1}^i}{2\Delta T_m}$$

$$\frac{\partial^2 p}{\partial T_m^2} = \frac{p_{n-1}^i - 2p_n^i + p_{n+1}^i}{\Delta T_m^2}$$

$$\frac{\partial p}{\partial T_m} = \frac{p^i_{n+1} - p^i_{n-1}}{2\Delta T_m} \tag{A1}$$

Substituting the finite difference derivatives (A1) in Eqs. (11) – (20), one can obtain a system of nonlinear equations which is solved using the *FSolve* function in MATLAB. As an example, Eq. (11) can be expressed as:

$$\frac{(M^i_n + 1)(U^i_{n-1} - 2U^i_n + U^i_{n+1})}{\Delta T_m^2} - \frac{E_A\left(\frac{(V^{i+1}_{n+1} - V^{i-1}_{n+1})(U^{i+1}_{n+1} - 2U^i_{n+1} + U^{i-1}_{n+1})}{2\Delta Y^3} + \frac{(U^{i+1}_{n+1} - U^{i-1}_{n+1})(V^{i+1}_{n+1} - 2V^i_{n+1} + V^{i-1}_{n+1})}{2\Delta Y^3}\right)}{L_D}$$

$$\frac{3(U^{i+1}_{n+1} - U^{i-1}_{n+1})^2(U^{i+1}_{n+1} - 2U^i_{n+1} + U^{i-1}_{n+1})}{4\Delta Y^4} + \frac{(V^{i+1}_{n+1} - V^{i-1}_{n+1})^2(U^{i+1}_{n+1} - 2U^i_{n+1} + U^{i-1}_{n+1})}{4\Delta Y^4} + \frac{(W^{i+1}_{n+1} - W^{i-1}_{n+1})^2(U^{i+1}_{n+1} - 2U^i_{n+1} + U^{i-1}_{n+1})}{4\Delta Y^4} +$$

$$\frac{(U^{i+1}_{n+1} - U^{i-1}_{n+1})(V^{i+1}_{n+1} - V^{i-1}_{n+1})(V^{i+1}_{n+1} - 2V^i_{n+1} + V^{i-1}_{n+1})}{2L_D\Delta Y^4} + \frac{(U^{i+1}_{n+1} - U^{i-1}_{n+1})(W^{i+1}_{n+1} - W^{i-1}_{n+1})(W^{i+1}_{n+1} - 2W^i_{n+1} + W^{i-1}_{n+1})}{2L_D\Delta Y^4}$$

$$\frac{T^i_{n_n}(U^{i+1}_{n+1} - 2U^i_{n+1} + U^{i-1}_{n+1})}{\Delta Y^2} + \frac{E_I(6U^i_{n+1} - 4U^{i+1}_{n+1} + U^{i+2}_{n+1} - 4U^{i-1}_{n+1} + U^{i-2}_{n+1})}{\Delta Y^4} - \frac{M^i_n(U^i_{n-1} - U^i_{n+1})}{2\Delta T_m} - \frac{T^i_{n_n}(U^{i+1}_{n+1} - U^{i-1}_{n+1})}{2\Delta Y} - \frac{\zeta(U^i_{n-1} - U^i_{n+1})}{\Delta T_m}$$

$$-\frac{C_d^-\left(\frac{Vr_i}{2p^i_n} + \frac{U^i_{n-1} - U^i_{n+1}}{2\Delta T_m}\right)\left(\left(\frac{Vr_i}{2p^i_n} + \frac{U^i_{n-1} - U^i_{n+1}}{2\Delta T_m}\right)^2 + \frac{(V^i_{n-1} - V^i_{n+1})^2}{4\Delta T_m^2} + \frac{(W^i_{n-1} - W^i_{n+1})^2}{4dT_m^2}\right)^{\frac{1}{2}}}{2mu} - \frac{M^i_n U_r(U^i_{n-1} - U^i_{n+1})}{2\Delta T_m}$$

$$+\frac{M^i_n U_r(U^{i+1}_{n+1} - U^{i-1}_{n+1})}{2\Delta Y} + \frac{M^i_n U_r^2(U^{i+1}_{n+1} - U^{i-1}_{n+1})}{2\Delta Y} + \frac{M^i_n U_r^2(U^{i+1}_{n+1} - 2U^i_{n+1} + U^{i-1}_{n+1})}{\Delta Y^2}$$

$$-\frac{C_{d0}p^i_n\left(\frac{Vr_i}{2p^i_n} + \frac{U^i_{n-1} - U^i_{n+1}}{2dT_m}\right)\left(\left(\frac{Vr_i}{2p^i_n} + \frac{U^i_{n-1} - U^i_{n+1}}{2dT_m}\right)^2 + \frac{(V^i_{n-1} - V^i_{n+1})^2}{4dT_m^2} + \frac{(W^i_{n-1} - W^i_{n+1})^2}{4dT_m^2}\right)^{\frac{1}{2}}}{4\mu}$$

$$-\frac{M^i_n U_r(U^{i+1}_{n-1} - U^{i-1}_{n-1} - U^{i+1}_{n+1} + U^{i-1}_{n+1})}{2\Delta T_m\Delta Y} + \frac{C_I q^i_n(W^i_{n-1} - W^i_{n+1})\left(\left(\frac{Vr_i}{2p^i_n} + \frac{U^i_{n-1} - U^i_{n+1}}{2dT_m}\right)^2 + \frac{(V^i_{n-1} - V^i_{n+1})^2}{4dT_m^2} + \frac{(W^i_{n-1} - W^i_{n+1})^2}{4dT_m^2}\right)^{\frac{1}{2}}}{8\Delta T_m\mu} \tag{A2}$$

The values at U^i_0, V^i_0, W^i_0, p^i_0, and q^i_0 can be obtained from the initial conditions of U, V, W equal to zero and wake variables p and q equal to 2. However, the initial conditions of $\frac{\partial U}{\partial T_m} = 0$, $\frac{\partial V}{\partial T_m} = 0$, $\frac{\partial W}{\partial T_m} = 0$, $\frac{\partial p}{\partial T_m} = 0$ and $\frac{\partial q}{\partial T_m} = 0$ must be used when determining the values at U^i_1, V^i_1, W^i_1, p^i_1 and q^i_1. From these initial conditions one can have:

$$U^i_{-1} = U^i_1$$

$$V^i_{-1} = V^i_1$$

$$W^i_{-1} = W^i_1$$

$$p^i_{-1} = p^i_1$$

$$q^i_{-1} = q^i_1 \tag{A3}$$

Substituting Eqs. (A3) into equations similar to (A2) will result in a new system of nonlinear equations which its solution will provide U^i_1, V^i_1, W^i_1, p^i_1 and q^i_1. A detailed description of this discretization method can also be found in Riley et al. (1998).

References

Al-Hashimy, Z.I., Al-Kayiem, H.H., Time, R.W., 2016. Experimental investigation on the vibration induced by slug flow in horizontal pipe. ARPN J. Eng. Appl. Sci. (11), 12134–12139.

Bordalo, S.N., et al., 2008. Whipping phenomenon caused by the internal flow momentum on the catenary risers of offshore petroleum fields. In: Proceedings of the ASME 27th International Conference on Offshore Mechanics and Artic Engineering, OMAE2008-57351, pp. 1–9. https://doi.org/10.1115/OMAE2008-57351.

Bowen, M., Srinil, N., 2020. Planar dynamics of inclined curved flexible riser carrying slug liquid-gas flows. J. Fluids. Struct. 94, 1–41. https://doi.org/10.1016/j.jfluidstructs.2020.102911.

Dai, H., Wang, L., Qian, Q., Ni, Q., 2013. Vortex-induced vibrations of pipes conveying fluid in the subcritical and supercritical regimes. J. Fluids. Struct. 39, 322–334. https://doi.org/10.1016/j.jfluidstructs.2013.02.015.

Ehinmowo, A.B., Cao, Y., 2015. Stabilizing slug flow at large valve opening using active feedback control. In: Proceedings of the 21st International Conference on Automation and Computing. Glasgow. https://doi.org/10.1109/IConAC.2015.7313973.

Facchinetti, M., Langre, E.d., Biolley, F., 2004. Coupling of structure and wake oscillators in vortex-induced vibrations. J. Fluid Struct. 19, 123–140. https://doi.org/10.1016/j.jfluidstructs.2003.12.004.

Gao, Y., et al., 2019. Numerical prediction of vortex-induced vibrations of a long flexible cylinder in uniform and linear shear flows using a wake oscillator model. Ocean Eng. 171, 157–171. https://doi.org/10.1016/j.oceaneng.2018.10.044.

Gong, Z., 2010. Explosion analysis of the steam pipeline. Guangzhou Chem. Ind. 38, 181–182.

Griffith, P., 1984. Multiphase flow in pipes. J. Petrol. Technol. 36 (03), 361–367.

Hara, F., 1973. A theory on the two-phase flow induced vibrations in piping systems. In: Transactions of the 2nd International Conference on Structural Mechanics in Reactor Technology, F 5/1, pp. 1–16.

Jia, D., 2012. Slug flow induced vibration in a pipeline span, a jumper and a riser section. In: Offshore Technology Conference. OTC. https://doi.org/10.4043/22935-MS. OTC-22935.

Jia, D., 2013. Effect of boundary conditions, flow rate, slug length, and slug frequency on slug flow induced vibration in a pipeline span. In: Offshore Technology Conference. OTC. https://doi.org/10.4043/24051-MS. OTC-24051.

Khan, U., Pao, W., Sallih, N., 2022. A review: factors affecting internal two-phase flow induced vibrations. J. Appl. Sci. 12 (8406), 1–23. https://doi.org/10.3390/app12178406.

Meng, S., Song, S., Che, C., Zhang, W., 2018. Internal flow effect on the parametric instability of deepwater risers. Ocean Eng. 149, 305–312. https://doi.org/10.1016/j.oceaneng.2017.12.031.

Meng, S., Chen, Y., Che, C., 2020. Slug flow's intermittent feature affects VIV responses of flexible marine risers. Ocean Eng. 5, 1–10. https://doi.org/10.1016/j.oceaneng.2019.106883.

Miranda, J.M.C., Paik, J.K., 2019. Two-phase flow induced vibrations in a marine riser conveying a fluid with rectangular pulse train mass. Ocean Eng. 174, 71–83. https://doi.org/10.1016/j.oceaneng.2019.01.044.

Moe, G., Chucheepsakul, S., 1988. The effect of internal flow on marine risers. In: Proceedings of the Seventh International Offshore Mechanics and Arctic Engineering Conference. Houston, USA, vol. 1, pp. 375–382, 1988.

Mohmmeda, A.O., Al-Kayiem, H.H., Nasif, M.S., Time, R.W., 2019. Effect of slug flow frequency on the mechanical stress behaviour of pipelines. Int. J. Pressure Vessels Piping 172, 1–9. https://doi.org/10.1016/j.ijpvp.2019.03.012.

Monette, C., Pettigrew, M.J., 2004. Fluid elastic instability of flexible tubes subjected to two-phase internal flow. J. Fluids. Struct. 19 (7), 943–956. https://doi.org/10.1016/j.jfluidstructs.2004.06.003.

Monprapussorn, T., Athisakul, C., Chucheepsakul, S., 2006. Nonlinear vibrations of an extensible flexible marine riser carrying a pulsatile flow. ASME. J. Appl. Mech. 74 (4), 754–769. https://doi.org/10.1115/1.2711226. July 2007.

Montoya-Hernández, D.J., Vázquez-Hernández, A.O., Cuamatzi, R., Hernandez, M.A., 2014. Natural frequency analysis of a marine riser considering multiphase internal flow behaviour. Ocean Eng. 92, 103–113.

Patel, M., Syed, F., 1989. Internal flow-induced behaviour of flexible risers. Eng. Struct 11, 266–280. https://doi.org/10.1016/0141-0296(89)90046-1.

Riley, K.F., Hobson, M.P., Bence, S.J., 1998. Mathematical methods for physics and engineering. Cambridge University Press, Cambridge. https://doi.org/10.1119/1.1921.

Song, J.N., Lu, L., Teng, B., Park, H.I., Tang, G.Q., Wu, H., 2011. Laboratory tests of vortex-induced vibrations of a long flexible riser pipe subjected to uniform flow. Ocean Eng. 38 (11–12), 1308–1322. https://doi.org/10.1016/j.oceaneng.2011.05.020.

Srinil, N., Wiercigroch, M., O'Brien, P., 2009. Reduced-order modelling of vortex-induced vibration of catenary riser. Ocean Eng. 36 (17–18), 1404–1414.

Srinil, N., 2010. Multi-mode interactions in vortex-induced vibrations of flexible curved/straight structures with geometric non-linearities. J. Fluids. Struct. 26, 1098–1122. https://doi.org/10.1016/j.jfluidstructs.2010.08.005.

Wallis, G.B., 1969. One-Dimensional Two-Phase Flow. McGraw-Hill.

Wang, L., Yang, Y., Li, Y., Wang, Y., 2018. Dynamic behaviours of horizontal gas-liquid pipes subjected to hydrodynamic slug flow: modelling and experiments. Int. J. Pressure Vessels Piping 161, 50–57. https://doi.org/10.1016/j.ijpvp.2018.02.005.

Wu, M.C., Lou, J.Y.K., 1991. Effects of rigidity and internal flow on marine riser dynamics. Appl. Ocean Res. 13 (5), 235–244. https://doi.org/10.1016/S0141-1187(05)80047-1.

Zaldivar, M., 2014. Quantification of flow rate during slug flow. SPEI flow assurance technical section.

Zanganeh, H., Srinil, N., 2016. Three-dimensional VIV prediction model for a long flexible cylinder with axial dynamics and mean drag magnifications. J. Fluids. Struct. 66, 127–146. https://doi.org/10.1016/j.jfluidstructs.2016.07.004.

Zanganeh, H., Kurushina, V., Srinil, N., 2021. iSLUG - Identification of Steady Slug Flow Characteristics. Newcastle University. Software. https://doi.org/10.25405/data.ncl.10006901.v1.

Zhu, H., Gao, Y., Zhao, H., 2018a. Experiment investigation on the flow-induced vibration of a free-hanging flexible riser by internal unstable hydrodynamic slug flow. Ocean Eng. 164, 488–507. https://doi.org/10.1016/j.oceaneng.2018.06.071.

Zhu, H., Zhao, H., Gao, Y., 2018b. Experimental investigation of vibration response of a free-hanging flexible riser induced by internal gas-liquid slug flow. Ocean Eng. 32, 633–645. https://doi.org/10.1007/s13344-018-0065-2.

Zhu, H., Gao, Y., Zhao, H., 2018c. Numerical prediction of vortex-induced vibrations of a long flexible cylinder in uniform and linear shear flows using a wake oscillator model. Ocean Eng. 171, 157–171. https://doi.org/10.1016/j.oceaneng.2018.10.044.